Au-Pd Separation Enhances Bimetallic Catalysis of Alcohol Oxidation

Xiaoyang Huang[#], Ouardia Akdim[#], Mark Douthwaite, Kai Wang, Liang Zhao, Richard J. Lewis, Samuel Pattisson, Isaac T. Daniel, Peter J. Miedziak, Greg Shaw, David J. Morgan, Sultan M. Althahban, Thomas E. Davies, Qian He, Fei Wang, Jile Fu, Donald Bethell, Steven McIntosh, Christopher J. Kiely and Graham J. Hutchings[*]

[*]*Corresponding author. E-mail: hutch@cardiff.ac.uk*

[#]*These authors contributed equally to this work.*

Max Planck- Cardiff Centre on the Fundamentals of Heterogeneous Catalysis FUNCAT, Cardiff Catalysis Institute, School of Chemistry, Cardiff University, Main Building, Park Place, Cardiff, CF10 3AT, United Kingdom.

Xiaoyang Huang, Ouardia Akdim, Mark Douthwaite, Liang Zhao, Kai Wang, Richard J. Lewis, Samuel Pattisson, Isaac T. Daniel, Peter J. Miedziak, Greg Shaw, David J. Morgan, Thomas E. Davies, Qian He, Fei Wang, Jile Fu, Donald Bethell and Graham J. Hutchings.

School of Applied Sciences, University of South Wales, Pontypridd, CF37 4AT (UK)

Peter J. Miedziak

Department of Materials Science and Engineering, Lehigh University, 5 East Packer Avenue, Bethlehem, PA 18015, USA.

Sultan M. Althahban, Christopher J. Kiely

Department of Mechanical Engineering, Jazan University, Jazan 82822, Saudi Arabia.

Sultan M. Althahban

Department of Materials Science and Engineering, Faculty of Engineering, National University of Singapore

Qian He

Department of Chemical and Biomolecular Engineering, Lehigh University, 111 Research Drive, Bethlehem, PA 18015, USA.

Steven McIntosh, Christopher J. Kiely

In oxidation reactions catalysed by supported metal nanoparticles with oxygen as the terminal oxidant, the rate of the oxygen reduction can be a limiting factor. This is exemplified by the oxidative dehydrogenation of alcohols, an important class of reactions with modern commercial applications[1–3]. For this reaction supported gold nanoparticles are very effective for the dehydrogenation of the alcohol to an aldehyde[4] but gold is less effective for oxygen reduction[5,6]. In contrast, supported palladium nanoparticles are less active for dehydrogenation but are active for oxygen reduction[5,6]. This imbalance can be overcome by alloying gold with palladium which gives enhanced activity to both reactions[7,8]; however, the electrochemical potential of the alloy is a compromise between that of the two metals meaning that although the oxygen reduction is improved in an alloy, the dehydrogenation activity is poorer. Here we show that by separating the gold and palladium components in bimetallic carbon-supported catalysts we can almost double the reaction rate beyond that achieved with a corresponding alloy catalyst. We demonstrate this using physical mixtures of carbon-supported monometallic Au and Pd and a bimetallic catalyst comprising separated gold and palladium regions. Furthermore, we demonstrate electrochemically that this enhancement is attributable to coupling of separate redox processes occurring at isolated gold and palladium sites. The discovery of this novel catalytic effect, a cooperative redox enhancement (CORE), offers a new approach to the design of multi-component heterogeneous catalysts.

Supported Au-Pd nanoalloys are effective catalysts for redox reactions[8] demonstrating rate enhancement compared with monometallic analogues, an effect referred to as synergy[8–14]. To date there has been no definitive demonstration of the origin of this effect, which we investigate for the oxidative dehydrogenation (ODH) of alcohols[14,15], using ODH of hydroxymethylfurfural (HMF) in aqueous alkaline solution as a model reaction to study the cooperative relation between Au and Pd nanoparticles.

Monometallic Au, Pd and a bimetallic Au and Pd catalyst (Au:Pd atomic ratio = 4), were synthesized using sol-immobilization[18] (Extended Data Fig. 1) and supported on Vulcan XC-72R carbon (C), denoted Au/C, Pd/C and Au-Pd/C, respectively. These catalysts were investigated for HMF oxidation and reacted as a slurry (Extended Data Fig 1e), as well as a physical mixture of Au/C and Pd/C (Figs. 1a, 1b and Extended Data Fig. 2) in aqueous $NaHCO_3$ (pH 8.7); the total moles of Au and Pd, and the mass of the carbon support were constant across

experiments. HMF conversion and product yields were monitored as a function of time with the monometallic Pd/C catalyst exhibiting a very limited activity over the duration of the experiment. Nonetheless, the initial rate of reaction, determined after 5 min over a physical mixture of the two monometallic catalysts was far greater ($k = 4.9 \times 10^{-5}$ $M.s^{-1}$) than that observed with the monometallic Au/C catalyst ($k = 2.5 \times 10^{-5}$ $M.s^{-1}$) and the monometallic Pd/C catalyst ($k = 2.7 \times 10^{-6}$ $M.s^{-1}$), which could therefore not be explained simply as an additive effect. Catalytic activity immediately increased after the addition of Pd/C to a reaction mixture containing Au/C (Extended Data Fig. 2f) and was not attributed to the addition of carbon alone (Extended Data Fig. 2g). Strikingly, the rate of HMF conversion in the presence of the Au/C and Pd/C physical mixture was greater than that observed over the Au-Pd/C alloy ($k = 3.8 \times 10^{-5}$ $M.s^{-1}$); an observation which has only been noted previously in an electrocatalytic study[16].

The differences in activity are further highlighted when the concentration of the terminal product formed (FDCA) is considered (Fig. 1b). The FDCA produced over the physical mixture, after 2 h of reaction, was almost 9.5 times greater than that produced over the Au/C catalyst. In multistep processes, such as this one, rate enhancements become multiplicative over sequential reactions. Thus, enhancement occurs when other oxygen-containing functionalities are oxidized. The trend in reactivity of these catalysts is amplified further when the estimated turnover frequencies (TOFs) of the materials are considered (Extended Data Fig. 2j).

We next investigated the ODH of the intermediates in HMF oxidation, 5-hydroxymethyl-2-furan carboxylic acid (HMFCA) and 5-formyl-2-furan carboxylic acid (FFCA), as well as a range of other alcohols, (Fig. 1c and Extended Data Fig. 3) observing the same trends in activity. Analysis of post-reaction solutions confirmed that these rate enhancements were not the result of metal leaching in any of the reactions, while STEM-XEDS confirmed no detectable metal migration occurred in reactions over the Au/C and Pd/C physical mixture (Extended Data Fig. 4).

We investigated a semiconducting support (TiO_2) and an insulating support (BN) to compare with the highly conducting XC72-R carbon support[17,18] (Fig. 1d, Extended Data Fig. 3e). With a physical mixture of Au/C and Pd/BN, the total yield of products formed was comparable to the sum generated in the reactions using Au/C and Pd/BN independently (Au/C+Pd/BN: 20.3%; Au/C: 17.9%; Pd/BN: 1.1%). When Pd/TiO_2 was combined with Au/C product yields notably greater than the sum of Au/C and Pd/TiO_2 independently were observed (Au/C+Pd/TiO_2:

29.2%; Au/C: 17.9%; Pd/TiO_2: 0.5%). Support effects in heterogeneous catalysis have many dimensions but these experiments show that the rate enhancement correlates well with the ability of the support material to accept and conduct electrons to and from the surface reaction sites. While TiO_2 provides limited conductivity and a conduction band edge at ~-0.37 V vs RHE for anatase structured TiO_2 that can accept electrons from the HMF oxidation step, the higher band gap of BN acts as a barrier to this transport.

Quantities of C, TiO_2 and BN were added to reactions containing physical mixtures of monometallic Au and Pd supported catalysts (Fig. 1e). The addition of C to a physical mixture of Au/TiO_2 and Pd/TiO_2, or BN supported analogues, resulted in a notable increase in catalytic reactivity based on the mass of C added. On the contrary, the addition of less conductive TiO_2, or non-conductive BN, to a physical mixture of Au/C and Pd/C led to a decrease in the rate of reaction; the suppression was greatest in the reactions where BN was added. Graphene nanoplatelets (30 mg) were added to a physical mixture of Au/TiO_2 and Pd/TiO_2 a greater enhancement in activity was observed, compared with the addition of C-XC72R, suggesting that other additive properties (in addition to conductivity) are likely to influence electron transport. Ultimately, these experiments suggest that substrate conversion over physical mixtures of Au and Pd monometallic catalysts can be enhanced through the incorporation of additives which are electronically conductive but are not by themselves catalytically active (Extended Data Fig. 3e). Further optimization and understanding of mitigating properties could undoubtedly lead to even greater activity enhancement. X-ray Photoelectron spectroscopy (XPS) and temperature programmed reduction (TPR) indicated that some Pd oxidation occurred during the reaction of a physical mixture of Au/C and Pd/C (Extended Data Fig. 5).

Hence, we propose a reaction scheme (Fig. 2) that explains the cooperative role of Au and Pd in alcohol and (hydrated) formyl oxidation reactions. Building on current understanding[16,19], we consider that the oxidation of HMF to HMFCA proceeds through a dehydrogenation reaction on the Au surface, which generates two protons in solution and two electrons that are transferred, *via* the support material, to Pd^{2+} where they are consumed in an oxygen reduction reaction (ORR); the catalytic cycle is completed by the rapid reaction in the liquid phase of the product hydroxide ions with protons. Increasing the pH of the reaction mixture affects the reaction rate by activating the substrate towards oxidation but not the electron-transfer mechanism. The oxidation of reaction intermediates HMFCA and FFCA are considered to proceed in the same way, terminating at FDCA. Alcohol oxidation over Au-supported catalysts is therefore proposed to be influenced by the rate of the coupled ORR occurring on Pd and the

ease with which electrons can migrate about the system, dictated to a large extent by the conductivity of the support employed. The lower activity observed over the Au-Pd/C catalyst can be explained by the change in the redox properties of Pd, when alloyed with Au[20]; the alloying of Au with Pd reduces the rate of the ORR on Pd sites. This hypothesis is further supported by additional testing data, which confirms that ODH on Au sites, is limited by ORR taking place on Pd sites (Extended Data Fig. 2h). Over a physical mixture of Au/C and Pd/C; as the mass of Pd/C is increased, and the mass of Au/C kept constant, a linear increase in ODH activity was observed, which could not be attributed to any direct contribution from the additional Pd or C present in the reaction. This also explains why the rate of reaction over both the monometallic Au/C catalyst and Au/C + Pd/C physical mixture is influenced by, but is not directly proportional to, O_2 pressure (Extended Data Fig. 2i). Oxygen pressure is proposed to influence the rate of ORR which, consequently, impacts the observed rate of ODH. Thus, the relationship between O_2 pressure and ODH activity is indirect and limited by other factors, such as electron transport (in the physical mixture) or competitive adsorption of substrate and O_2 (in the monometallic Au catalyst). It should however be noted that this enhancement, as O_2 pressure is increased, could be attributed to gas/liquid mass transfer, and requires further exploration.

To confirm the critical role of the electron transfer, analogous electrocatalytic experiments were performed. The electrocatalytic oxidation of HMF is well-established and the trend observed in peak current density from cyclic voltammetry (Fig. 3a) for the Au/C, Pd/C and Au-Pd/C catalysts aligns with previous literature[21]. The trend in electrocatalytic current density across the catalysts correlates strongly with the trend in thermal catalytic rate (Extended Data Fig. 6a).

Electron transfer between Au/C and Pd/C was demonstrated by externally short-circuiting Au/C and Pd/C electrodes together in a single-chamber cell. Under aerobic conditions (Fig. 3b and Extended Data Fig. 6c), current was measured to flow from the Au/C electrode to the Pd/C electrode. The drop in current was attributed to the mass-transfer limitation of oxygen from the solution to Pd electrode interface. The current density was near zero in the absence of HMF. A control reaction where replacing Pd/C by C, showed a drastic decrease in the current density (from 715 $\mu A/cm^2$ to 239 $\mu A/cm^2$ at 30 min;), demonstrating the critical role of Pd as a reaction partner in consuming electrons generated by HMF oxidation on Au/C. Repeated switching between nitrogen and oxygen atmosphere in the cell every 60 min led to concomitant switching

of the current density between approximately 100 μA/cm^2 and 600 μA/cm^2 (Fig. 3b), demonstrating the essential role of oxygen in the electrocatalytic reaction.

Linear sweep voltammetry of Au/C and Pd/C electrodes under oxygen within the potential window reported for the ORR[22] was performed in the absence and presence of HMF (Fig. 3c). In the absence of HMF, both Pd and Au showed clear reduction peaks at 0.72 V, attributable to the ORR. However, the ORR peak current of Au/C decreased substantially in the presence of HMF, but that of Pd/C was largely unaffected. This suggests that under reaction conditions the Au sites predominantly catalyse dehydrogenation, whereas Pd sites continue to catalyse oxygen reduction. The mechanistic role of electron transfer between the metals was further demonstrated using a dual chamber electrochemical cell where the Au/C and Pd/C electrodes were physically separated by an anion exchange membrane, but electrically connected via an external circuit, with Au and Pd electrodes under an atmosphere of N_2 and O_2, respectively (Figs. 3d and Extended Data Fig. 6d). The short-circuit current between the electrodes was measured over time while monitoring the HMF conversion and selectivity in the Au/C chamber. The total molar electron transfer between the electrodes was then compared with that expected from HMF oxidation stoichiometry to determine the fraction of the ORR reaction occurring through a cooperative electron transfer from the Au/C to Pd/C. With identical weight loadings of Au and Pd on their respective electrodes, 65% of the ORR reaction occurred by electron transfer from Au/C to Pd/C, increasing to 82% upon doubling the Pd loading. It has been demonstrated that: (i) no current was generated in the absence of HMF; (ii) Au under N_2 alone demonstrated low activity toward HMF conversion; and (iii) the yield of HMFCA was substantially decreased if the two electrodes were not electrically connected in the dual chamber cell (Extended Data Fig 6e). These electrochemical experiments identify the role of each metal and the nature of these cooperative redox enhancement effects (CORE), supporting our hypothesis that the observed enhancement occurred through physical separation of catalytic function which was critically facilitated by electrical connectivity through the support.

Interestingly, the activity of a material possessing spatially separated Au and Pd nanoparticles on the same support grain for HMF ODH (denoted Au=Pd/C with morphology confirmed by STEM-XEDS, Extended Data Fig. 7) was identical to that of the physical mixture, an effect we consider is due to the highly conducting nature of the carbon support as demonstrated in the experiments where we have added additional carbon (Fig. 1e)

As we concluded that spatially separating the Au and Pd provides the origin of the rate enhancement, we reasoned that synthesizing nanoparticles comprising phase separated Au and Pd regions within single nanoparticles, *i.e.* not alloyed, would provide an even greater rate enhancement. We therefore synthesised small clusters of Pd situated on the surface of Au nanoparticles (Janus-like nanoparticles) denoted Au@Pd/C (Figs. 4j-l). This is evidenced through comparison with micrographs of the Au/C catalyst (Figs. 4a-c) and is in stark contrast to the particles present in the alloyed Au-Pd/C catalyst (Figs. 4g-i). The material was evaluated in the thermocatalytic reactions (Figs. 1a, 1b and 1c) and probed by cyclic voltammetry (Fig. 3a). In both cases, increased activity was observed, as predicted by our proposed model.

The validity of this concept was further evidenced when performance of the Au@Pd/C catalyst and a physical mixture of Au/C and Pd/C catalysts was assessed over multiple uses. For the Au@Pd/C sample we noted a slight loss in activity after use, which we consider was due to the formation of some surface AuPd alloy (Extended Data Fig. 8), which correlated with a decrease in catalytic activity over subsequent uses (Extended Data Figs. 9 a, b). Analogous STEM-XEDS analysis of the used Au/C + Pd/C sample after reaction as a physical mixture, confirmed that there was no detectable metal migration or alloying (Extended Data Fig. 4). This correlated with the reactivity data as the performance of the Au/C + Pd/C physical mixture remained stable over three uses (Extended Data Figs. 9 c, d). The loss of catalytic activity with the formation of some alloy in the Au@Pd/C sample after several uses further strengthens our view of the role of Au in inhibiting the redox properties of Pd; as a higher proportion of Pd becomes alloyed with Au, the rate of the Pd redox cycle would also be diminished and hence its activity for the ORR.

It would appear that by removing the need for electron transfer to occur through the carbon support, thus reducing any potential resistance, the reactivity of towards ODH on the Au sites could be further increased. However, it should be noted that, in general, the Pd particles present in the Au@Pd/C catalyst are smaller than those present in the analogous Pd/C catalyst (extended data Fig7d). Whilst we suspect these smaller Pd particles would provide less of a contribution towards direct ODH, it's likely that the change in particle size would also influence ORR rate, which we have confirmed to be rate limiting for ODH (extended data Fig. 2h).

While we recognize that there are some mechanistic features that we have not yet fully addressed, we consider that for the oxidations described the active sites on the Au and Pd

nanoparticles work through redox cooperation. This CORE effect, controlled largely by electron transfer, as opposed to molecular transport, is a wholly new observation in heterogeneous catalysis and requires a conductive support; the electrochemical experiments are consistent with this view. We propose that the rate of the Pd redox cycle and ease with which electrons can migrate about the system ultimately dictates the intrinsic catalytic activity observed. For HMF oxidation, the primary model reaction studied, our Au@Pd/C catalyst is among the most active reported to date (Extended data Table 1). We consider that the discovery of CORE effects will provide an additional dimension to research into bimetallic catalysts and provides a new foundation for the development of multi-component heterogeneous catalysts.

Main References

1. Mallat, T. & Baiker, A. Oxidation of alcohols with molecular oxygen on solid catalysts. *Chem. Rev.* **104**, 3037–3058 (2004).

2. Ciriminna, R., Pandarus, V., Béland, F., Xu, Y. J. & Pagliaro, M. Heterogeneously catalyzed alcohol oxidation for the fine chemical industry. *Org. Process Res. Dev.* **19,** 1554–1558 (2015).

3. Sheldon, R. A., Arends, I. W. C. E., Brink, G. J. Ten & Dijksman, A. Green, catalytic oxidations of alcohols. *Acc. Chem. Res.* **35**, 774–781 (2002).

4. Abad, A., Concepción, P., Corma, A. & García, H. A collaborative effect between gold and a support induces the selective oxidation of alcohols. *Angew. Chem. Int. Ed.* **44**, 4066–4069 (2005).

5. Kulkarni, A., Siahrostami, S., Patel, A. & Nørskov, J. K. Understanding catalytic activity trends in the oxygen reduction reaction. *Chem. Rev.***118**, 2302–2312 (2018).

6. Nørskov, J. K. *et al.* Origin of the overpotential for oxygen reduction at a fuel-cell cathode. *J. Phys. Chem. B* **108**, 17886–17892 (2004).

7. Zhu, X. *et al.* Optimising surface d charge of AuPd nanoalloy catalysts for enhanced catalytic activity. *Nat. Commun.* **10**, 1428 (2019).

8. Enache, D. I. *et al.* Solvent-free oxidation of primary alcohols to aldehydes using Au-Pd/TiO2 catalyst. *Science* **311**, 362–365 (2006).

9. Hutchings, G. J. & Kiely, C. J. Strategies for the synthesis of supported gold palladium nanoparticles with controlled morphology and composition. *Acc. Chem. Res.* **46**, 1759–1772 (2013).

10. Wang, A., Liu, X. Y., Mou, C. Y. & Zhang, T. Understanding the synergistic effects of gold bimetallic catalysts. *J. Catal.* **308**, 258–271 (2013).

11. Wang, D., Villa, A., Porta, F., Prati, L. & Su, D. Bimetallic gold/palladium catalysts: Correlation between nanostructure and synergistic effects. *J. Phys. Chem. C* **112**, 8617–8622 (2008).

12. Gao, F. & Goodman, D. W. Pd-Au bimetallic catalysts: Understanding alloy effects from planar models and (supported) nanoparticles. *Chem. Soc. Rev.* **41**, 8009–8020 (2012).

13. Han, S. & Mullins, C. B. Catalytic Reactions on Pd-Au Bimetallic Model Catalysts. Acc. Chem. Res. **54**, 379–387 (2021).

14. Davis, S. E., Ide, M. S. & Davis, R. J. Selective oxidation of alcohols and aldehydes over supported metal nanoparticles. *Green Chem.* **15**, 17–45 (2013).

15. Parmeggiani, C., Matassini, C. & Cardona, F. A step forward towards sustainable aerobic alcohol oxidation: New and revised catalysts based on transition metals on solid supports. *Green Chem.***19**, 2030–2050 (2017).

16. Suo, Y., Zhuang, L. & Lu, J. First-principles considerations in the design of Pd-alloy catalysts for oxygen reduction. *Angew. Chem. Int. Ed.* **46**, 2862–2864 (2007).

17. Pelaez, M. *et al.* A review on the visible light active titanium dioxide photocatalysts for environmental applications. *Appl. Catal. B* **125**, 331–349 (2012).

18. Golberg, D. *et al.* Boron nitride nanotubes and nanosheets. *ACS Nano* **4**, 2979–2993 (2010).

19. Zope, B. N., Hibbitts, D. D., Neurock, M. & Davis, R. J. Reactivity of the gold/water interface during selective oxidation catalysis. *Science* **330**, 74–78 (2010).

20. Han, Y. F. *et al.* Au promotional effects on the synthesis of H_2O_2 directly from H_2 and O_2 on supported Pd-Au alloy catalysts. *J. Phys. Chem. C* **111**, 8410–8413 (2007).

21. Chadderdon, D. J. *et al.* Electrocatalytic oxidation of 5-hydroxymethylfurfural to 2,5-

furandicarboxylic acid on supported Au and Pd bimetallic nanoparticles. *Green Chem.* **16**, 3778–3786 (2014).

22. Zhu, Y. *et al.* Boosting oxygen reduction reaction activity of palladium by stabilizing its unusual oxidation states in perovskite. *Chem. Mater.* **27**, 3048–3054 (2015).

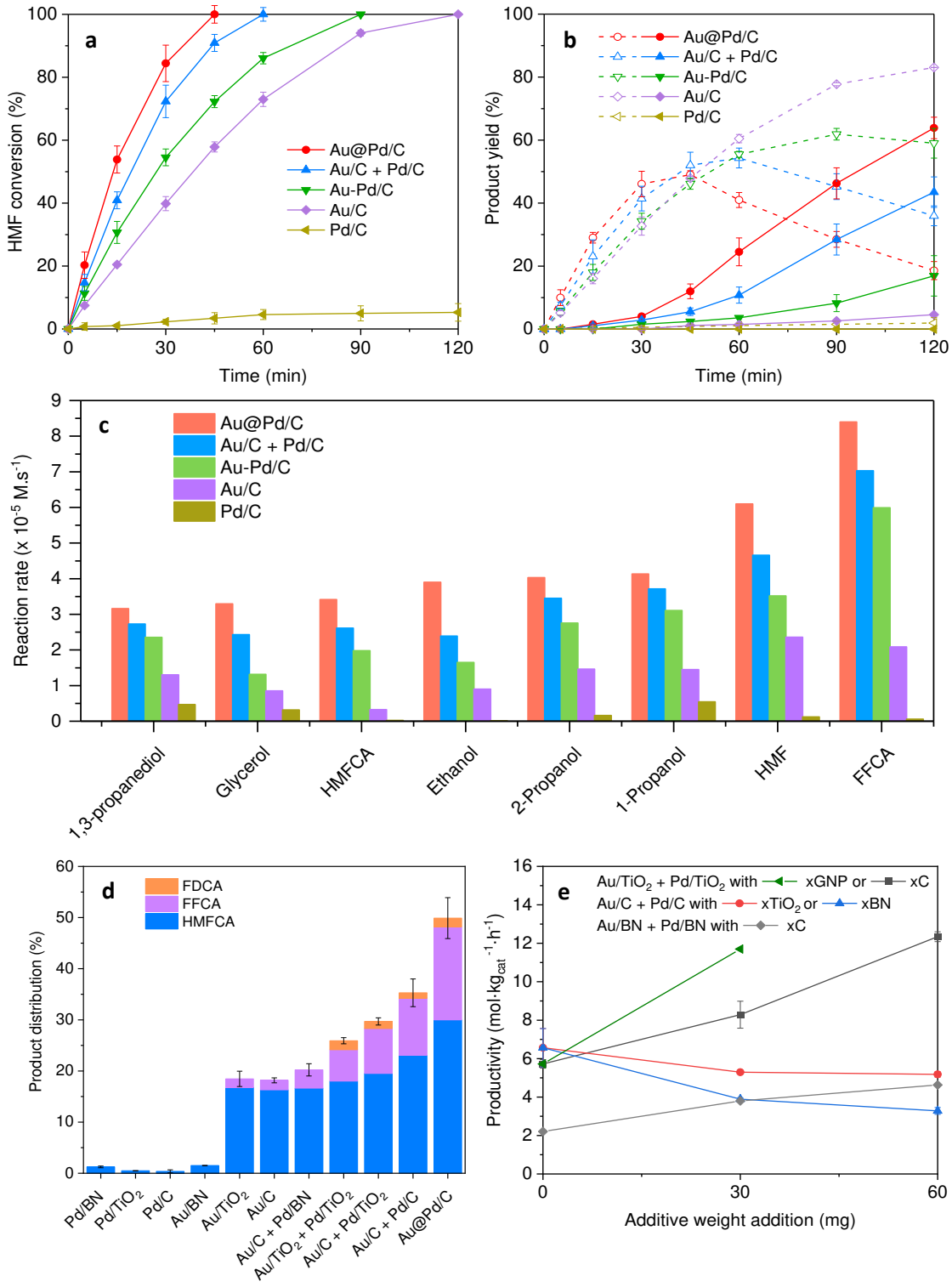

Figure 1. Catalytic performance for aqueous HMF oxidation. **a**, HMF conversion and **b**, product yield of HMFCA (dashed line) and FDCA (solid line) as a function of time over a series of catalytic formulations. Reaction conditions: HMF (0.1 M); $NaHCO_3$ (0.4 M); H_2O (16 mL); 80 °C; pO_2 = 3 bar; catalyst amounts for Au@Pd/C, Au/C + Pd/C and Au-Pd/C: 143.1 mg; Au/C: 72.1 mg; Pd/C and carbon: 71 mg. For each reaction, the moles of Au and Pd used are always constant (Au/Pd = 4 (mol/mol)). Associated error bars correspond to mean +/- SD (N = 5). **c**, Rates of reaction displayed by each of the catalysts for the aqueous phase aerobic oxidation of formyls (HMF and FFCA) and a number of simple alcohols, under alkaline conditions. Further details relating to the reaction conditions used can be found in the Method section. Influence of support on the catalytic performance of various physical mixtures containing Au and Pd for HMF oxidation. **d**, Product yield distribution

for aqueous oxidation of HMF over physical mixtures of different catalysts or supports. Reaction conditions: HMF (0.1 M); $NaHCO_3$ (0.4 M); H_2O (16 mL); 80 °C; Au/C + Pd/C and Au-Pd/C: 143.1 mg; Au/C: 72.1 mg; Pd/C and carbon: 71 mg. For each reaction, the moles of Au and Pd used are always constant (Au/Pd = 4 (mol/mol)). Associated error bars correspond to mean +/- SD (N = 5). Rates of reaction displayed by each of the catalysts for the aqueous phase aerobic oxidation of pO_2 = 3 bar; supported Au catalyst (72.1 mg); supported Pd catalyst (71 mg); reaction time: 15 min. **e**, The addition of increasing amounts of either C, GNP, TiO_2 or BN to various physical mixtures and its effect on productivity. Supported Au catalyst (15 mg); supported Pd catalyst (15 mg); reaction time: 30 min. Note: The moles of Au and Pd used are always constant (Au/Pd = 4 (mol/mol)). Associated error bars correspond to mean +/- SD (N = 3).

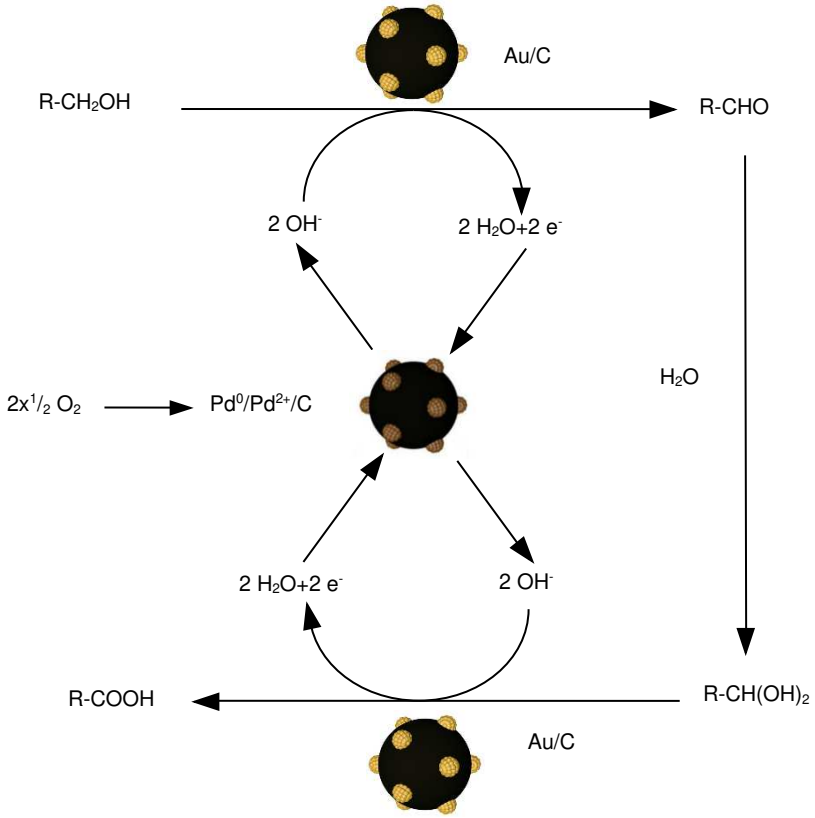

Figure 2. Proposed reaction scheme for the aqueous phase oxidation of alcohols and formyls over a physical mixture of Au/C and Pd/C. A CORE is facilitated by ORRs taking place on Pd sites.

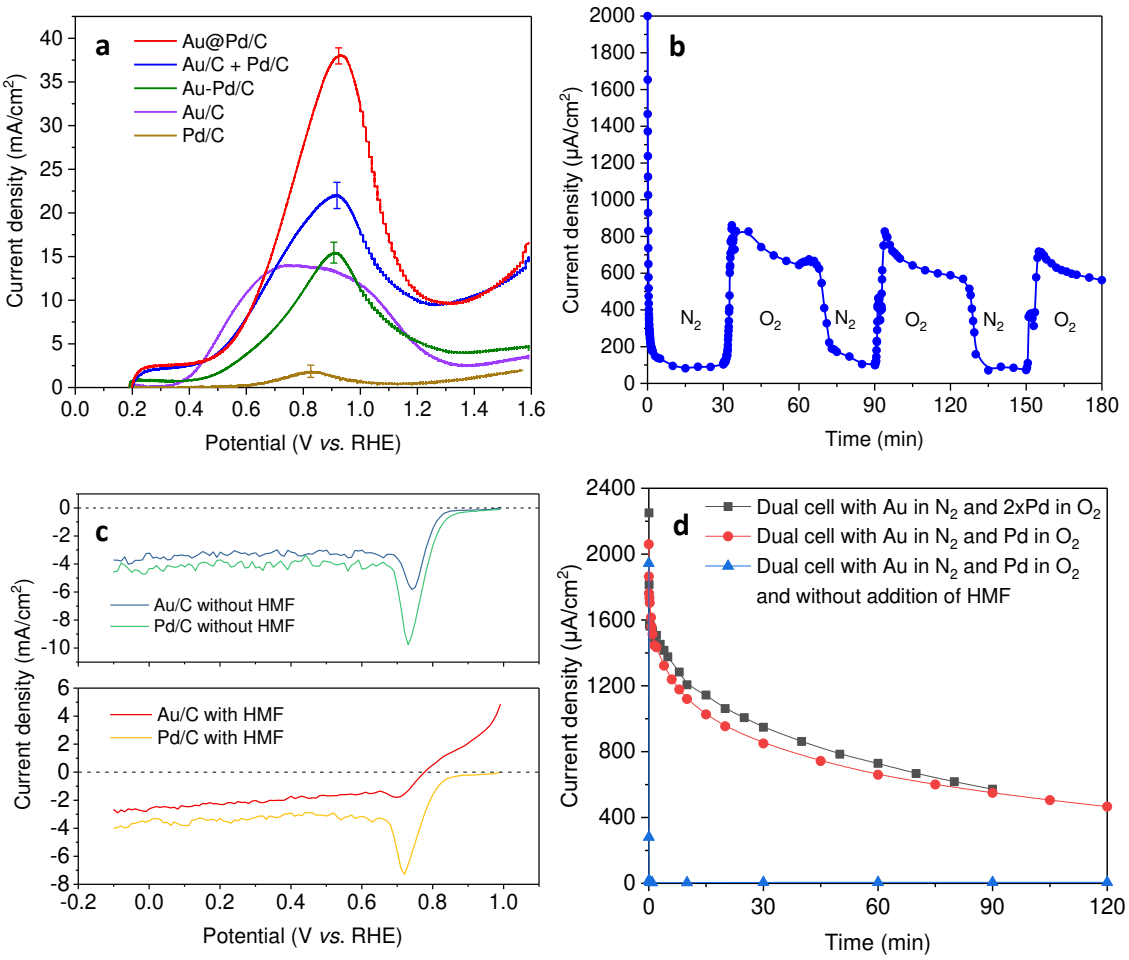

Figure 3. Electrocatalytic performance. a, Cyclic voltammetry (anodic scan) of half-cell with HMF solution. Net current density is the difference between anodic-scan current density and blank current density (0.1 M NaOH only). Reaction conditions: 0.1 M NaOH; 0.02 M HMF; 50 mL H_2O; 25 °C; scan rate 50 $mV \cdot s^{-1}$; N_2 flow: 50 mL/min. **b**, Short circuit with current generated as a function of time in the single cell. Reaction conditions: 0.1 M NaOH and 0.02 M of HMF in 50 mL H_2O; Au (working electrode) and Pd (counter electrode); 25 °C; a 30 min periodic switch between N_2 and O_2 with a flow of 50 mL/min. **c**, ORR polarization curves for Au/C and Pd/C monometallic catalysts with and without HMF being present. Reaction conditions: 0.1 M NaOH and 0.02 M of HMF (or without) in 50 mL H_2O; 25 °C; O_2 flow: 50 mL/min. **d**, Short circuit with current generated as a function of time in the dual cell. Reaction conditions: each cell consists of 0.1 M NaOH and 0.02 M of HMF in 35 mL H_2O; Au (working electrode under N_2) or Pd (counter electrode under O_2); 25 °C; O_2/N_2 flow: 50 mL/min. Note: The molar ratio of Au and Pd used is always constant (Au/Pd = 4 (mol/mol)). Associated error bars correspond to mean +/- SD (N = 3).

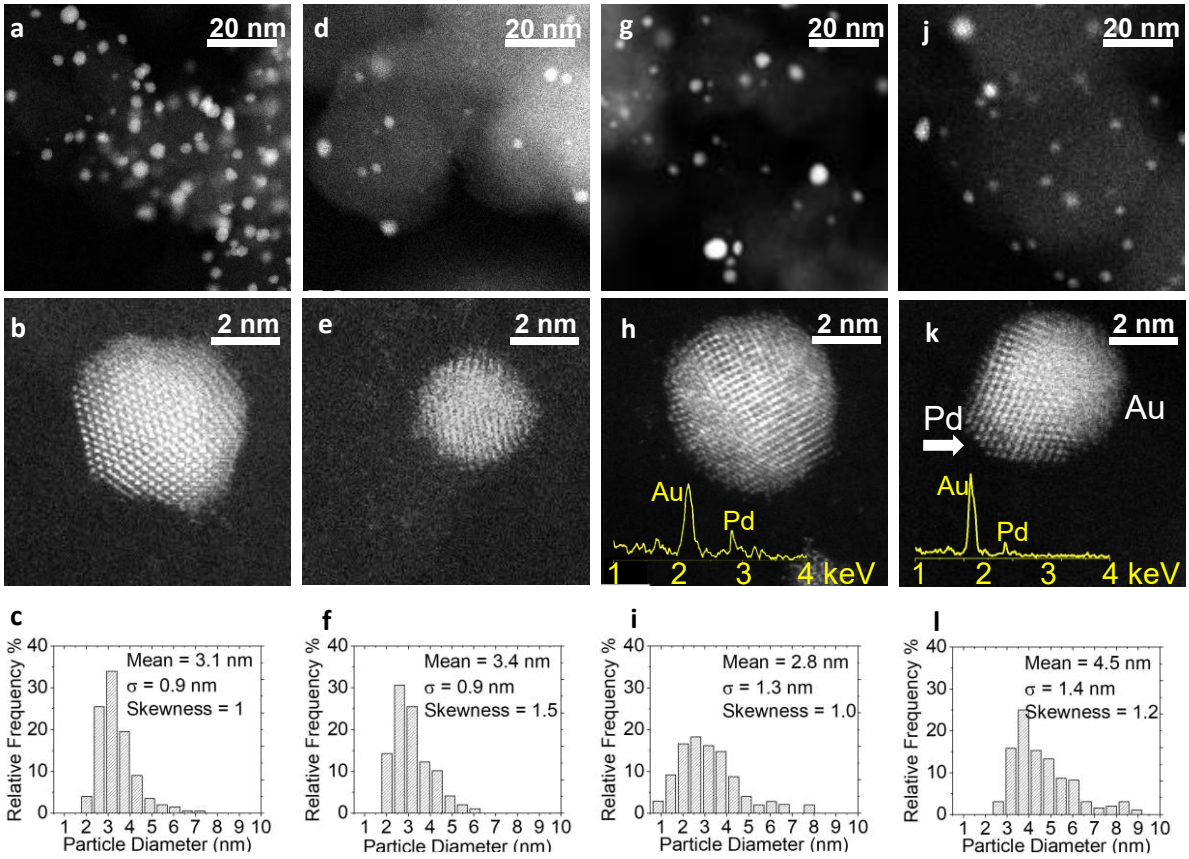

Figure 4. Representative STEM-HAADF images and the corresponding particle size distribution. **a**-**c**, Au/C; **d**-**f**, Pd/C; **g**-**i**, Au-Pd/C and **j**-**l**, Au@Pd/C catalysts. The inset shown in images h and k are the XEDS spectra of the corresponding particle, showing the presence of peaks of Au M (~2.1keV) and Pd L (~2.8keV). Image k highlight a Janus-like nanoparticle morphology. The Pd side is highlighted with a white arrow.

Methods

Chemicals (Source, Purity)

Acetic acid (Sigma Aldrich, > 99.7%); Boron Nitride (Sigma Aldrich, powder, 98%); Chloroauric acid (Strem Chemicals, 99.8%); Distilled water millipore (18.2 MΩ.cm at 25°C); Ethanol (Fisher Scientific, > 99%); 5-Formyl-2-furoic-acid (Tokyo Chemical Industry, > 98%); Glycerol (Sigma Aldrich, > 99.5%); Graphene nanoplatelets (Alfa Aesar); Hydroxymethylfurancarboxylic acid (Carbosynth, > 97%); 5-Hydroxymethylfurfural (Sigma Aldrich, > 99%); 2,5-Furandicarboxylic acid (Sigma Aldrich, 97 %); Molecular O_2 (BOC, > 99.95%); Nafion (Sigma Aldrich, 5 wt.% in lower aliphatic alcohols and water, contains 15-20% water); Palladium Chloride (Sigma Aldrich, > 99.9%); Polyvinyl Alcohol (Sigma-Aldrich, 80 % hydrolyzed); 1-Propanol (Sigma Aldrich, anhydrous, 99.7%); 2-Propanol (Sigma Aldrich, anhydrous, 99.5%); 1,3-Propanediol (Sigma Aldrich, > 99.6%); Sodium bicarbonate (Fisher Scientific, > 99.5%); Sodium Borohydride (Sigma-Aldrich, 99.99 %); Sodium carbonate (Fisher Scientific, > 99.5%); Titanium dioxide – P25 (Degussa, ≥ 99.5%); Vulcan XC72R (Cabot Corporation).

Materials Preparation

Synthesis of 1.75 wt.% Au/C, 0.25 wt.% Pd/C and 1wt.% Au-Pd/C catalysts by sol-immobilisation. Aqueous solutions of the metal precursors, $PdCl_2$ (10 mg/mL) or $HAuCl_4.3H_2O$ (12.25 mg/mL), were added to H_2O (140 mL) and stirred vigorously. Polyvinyl alcohol (PVA) (mass of PVA / mass of Au, Pd or Au and Pd = 1/1) is subsequently added to the solution. A freshly prepared $NaBH_4$ solution (0.15 M, $NaBH_4$ / total metal = 4/1, mole/mole) was added to the solution immediately, forming a sol. After this, the support material was added (0.5 g) was added to the colloidal solution with stirring facilitating the immobilisation of the metal nanoparticles. After 30 min, the solid catalyst was recovered by filtration and washed repeatedly with 500 mL distilled water to remove Na^+, BH^-_4 and BO^-_2. Finally, the catalysts were dried at 110 °C for 16 h under static air. Schematic representations of these synthesis methods are listed in Extended Data Fig. 1.

Synthesis of the 1 wt.% Au@Pd/C catalyst by sol-immobilization. The procedure used for the synthesis of this material is similar to that listed in the previous section. However, for the synthesis of this catalyst, Au and Pd colloids were prepared separately. The metal precursors were combined with analogous quantities of PVA and reduced with an analogous quantity of

$NaBH_4$, in separate beakers. Once the colloids had been synthesized, they were combined into one beaker and the desired quantity of support is immediately added. After 30 min, the solid catalyst was recovered by filtration and washed repeatedly with 500 mL distilled water to remove Na^+, BH^-_4 and BO^-_2. Finally, the catalysts were dried at 110 °C for 16 h under static air. A schematic representation of this preparation is also shown in Extended Data Fig. 1.

Synthesis of the 1 wt.% (Au=Pd)/C catalyst by sol-immobilization. The procedure used for the synthesis of this material is similar to that listed in the above section, but with a two-step sequential reduction. Firstly, Pd/C was synthesized by adding $PdCl_2$ solution to 140 mL of H_2O, followed with addition of analogous quantities of PVA and $NaBH_4$, and 1 g of carbon. This Pd/C catalyst was recovered by filtration, washed repeatedly with 500 mL distilled water, and then dried at 110 °C for 16 h under static air. Secondly, (Au=Pd)/C was synthesized by adding $HAuCl_4.3H_2O$ solution to 140 mL of H_2O, followed with addition of analogous quantities of PVA and $NaBH_4$, and previously obtained Pd/C as support. This (Au=Pd)/C was recovered by filtration, washed repeatedly with 500 mL distilled water, and then dried at 30 °C for 16 h in a vacuum oven.

Catalyst Testing

Testing of catalysts in thermocatalytic experiments. The majority of the thermocatalytic testing in this work utilized HMF as the substrate. HMF oxidation was carried out in a glass Colaver reactor (50 mL). In a typical reaction, an aqueous solution (16 mL) consisting of HMF (0.1 M) and $NaHCO_3$ (0.4 M) was heated to 80 ˚C under constant stirring (1000 rpm). After temperature stabilization was achieved, the catalyst(s) (HMF/metal=200/1, mol/mol) was added and the reactor was purged with O_2 five times before the reaction was typically run for 2 h. The reaction was conducted under atmosphere of 3 bar O_2, this was continually fed in a semi-batch manner to maintain a constant head pressure in the reactor. Re-use experiments were also conducted for some of the catalysts. For this, the catalyst was removed and washed with deionised water (500 mL) and acetone (250 mL) after each experiment, dried at 110 °C for 16 h before being re-used in the experiment. Analyses and quantification of post reaction solutions was carried out using a high-performance liquid chromatography (Agilent Technologies 1200 series) equipped with a diode array detector. A Hi-Plex H (300 x 7.7 mm) column was used to separate the products with 5 mM aqueous H_2SO_4 solution as the mobile phase, at a flow rate of 0.7 mL/min. The conversion of HMF and the yield of each product were obtained directly using calibration curves of known concentrations.

Thermocatalytic experiments were also conducted on other substrates. The conditions used for these additional experiments varied and were selected through consideration of the conditions used for studies in the literature. The conditions used for testing of the additional substrates (glycerol, ethanol, 1-propanol, 2-propanol, 1,3-propanediol, HMFCA, FFCA) are listed below:

1-propanol oxidation: 1-propanol (0.4 M); Na_2CO_3 (1.2 M); H_2O (16 mL); 70 °C; pO_2 = 3 bar; 2 h; catalyst amounts for Au@Pd/C, Au/C + Pd/C and Au-Pd/C: 143.1 mg; Au/C: 72.1 mg; Pd/C: 71 mg.

2-propanol oxidation: 2-propanol (0.4 M); Na_2CO_3 (1.2 M); H_2O (16 mL); 70 °C; pO_2 = 3 bar; 2 h; catalyst amounts for Au@Pd/C, Au/C + Pd/C and Au-Pd/C: 143.1 mg; Au/C: 72.1 mg; Pd/C: 71 mg.

1,3-propanediol: 1,3-propandiol (0.4 M); Na_2CO_3 (1.2 M); H_2O (16 mL); 70 °C; pO_2 = 3 bar; 2 h; catalyst amounts for Au@Pd/C, Au/C + Pd/C and Au-Pd/C: 143.1 mg; Au/C: 72.1 mg; Pd/C: 71 mg.

HMFCA oxidation: HMFCA (0.1 M); $NaHCO_3$ (0.4 M); H_2O (16 mL); 80 °C; pO_2 = 3 bar; 1 h; catalyst amounts for Au@Pd/C, Au/C + Pd/C and Au-Pd/C: 143.1 mg; Au/C: 72.1 mg; Pd/C: 71 mg.

FFCA oxidation: FFCA (0.1 M); $NaHCO_3$ (0.4 M); H_2O (16 mL); 80 °C; pO_2 = 3 bar; 15 min; catalyst amounts for Au@Pd/C, Au/C + Pd/C and Au-Pd/C: 143.1 mg; Au/C: 72.1 mg; Pd/C: 71 mg.

HMF oxidation (Extended Data Fig. 2h): HMF (0.1 M); $NaHCO_3$ (0.4 M); H_2O (16 mL); 80 °C; pO_2 = 3 bar; 30 min; Au/C (72.1 mg, when employed); Pd/C (mass varied from 0 to 260 mg); Carbon (mass varied from 140 to 260 mg).

HMF Oxidation (Extended Data Fig. 2i): HMF (0.1 M); $NaHCO_3$ (0.4 M); H_2O (16 mL); 80 °C; pO_2 = 0.6 - 3 bar; 30 min; catalyst amounts for Au/C + Pd/C (Au/C: 72.1 mg; Pd/C: 71 mg) and Au/C (72.1 mg).

Given that in some of the reactions where initial rates were monitored we working at high conversion, we used a different activity calculation for substrate turned over ($Activity_{STO}$). Given that HMF oxidation to FDCA is a sequential reaction whereby the substrate undergoes sequential dehydrogenation reactions, it accounts for multiple turnovers. The equations used to calculate are listed below:

$$Activity_{STO} = \frac{(moles\ of\ HMFCA\ \times 1) + (moles\ of\ FFCA\ \times 2) + (moles\ of\ FDCA\ \times 3)}{time\ (s)}$$

$Activity_{STO}$ is used to present catalyst performance in Extended Data Figs. 2(h) and 2(i)

$$Productivity\ = \frac{(moles\ of\ HMFCA\ \times 1) + (moles\ of\ FFCA\ \times 2) + (moles\ of\ FDCA\ \times 3)}{mass\ of\ catalyts\ (kg)\ \times\ time\ (h)}$$

Productivity was used to present catalyst performance in Fig. 1(e)

Testing of catalysts by electrochemical experiments. An experimental procedure detailing how the catalysts were deposited onto the working electrode is listed below:

i. A catalyst ink was made by adding 0.007 g of the monometallic or 0.014 g of the bimetallic catalysts into 1 mL distilled water mixed with 0.1 mL Nafion solution.
ii. The prepared ink solution was then sonicated for 150 s.
iii. 0.02 mL of the ink was dropped onto the surface of the glassy carbon electrode (surface area: 0.07065 cm^2) which was then left to dry at room temperature for 16 h.
iv. The final amount of catalyst on the surface of the glassy carbon electrode was $1.27*10^{-4}$ g for the monometallic and $2.55*10^{-4}$ g for the bimetallic systems.

Cyclic voltammetry experiments were performed under an N_2 atmosphere, with N_2 bubbled continuously (150 mL/min) through the base electrolyte (0.11 M NaOH in 45 mL DI water) solution for 20 min prior to recording measurements. A Pt wire (7.5 cm long and 0.5 mm diameter 99.95% purity, from BASinc) was used as the counter electrode and a saturated calomel electrode (RE-2BP, ALS, Japan) was used as the reference electrode. The working electrode was first reduced at a fixed negative potential (-1.0 V) for 10 s to clean the surface. A background was then recorded with NaOH electrolyte for 3 cycles (-0.8 V-0.6 V) under nitrogen. Then HMF solution (5 mL, 0.2 M) was subsequently added into the base electrolyte solution and the CV traces were recorded for an additional 3 cycles (-0.8 V-0.6 V). All the experiments were conducted at a scan rate of 50 mV/s at room temperature with stirring and the third and final cycle was used for comparison.

Linear sweep voltammetry (LSV) experiments were carried out by bubbling N_2 through the electrolyte solution for 5 min before again conducting an electrode surface cleaning step; achieved through holding the electrode at -1.0V for 10 s. O_2 was subsequently bubbled through the electrolyte solution (150 mL/min) for 30 min, before running the LSV experiments. All the

experiments were conducted from -1.1 V to 0 V at a scan rate of 10 mV/s at room temperature, while stirring. All reported current densities are normalized by the electrode surface area of 0.07 cm^2.

A series of additional experiments were also conducted to assess electron transfer between Au and Pd components. For this, Au/C and Pd/C catalysts were deposited separately onto the surface of two glassy carbon electrodes following the same procedure described previously. Two kinds of cells were used for these experiments; a single chamber cell and a dual chamber cell. For the single chamber experiments, oxygen was bubbled through the electrolyte solution for 20 min at a flow rate of 150 mL/min, before the start of the experiment. The two electrodes were introduced through the cap of the reactor into the reaction solution while the solution oxygen was still flowing and a blank run was performed with a base electrolyte (0.1 M NaOH in 50 mL DI water), by connecting the electrodes through a shorted multi-meter. O_2 was then bubbled into the solution at 50 mL/min, while the current was recorded by a digital multimeter (25XT, Wavetek Meterman, 0.5% accuracy). All the reactions with HMF were carried out under the same conditions as the blank, but with the addition 0.1 M HMF to the electrolyte solution. At the end of each experiment a 0.4 mL of the electrolyte solution was collected and analysed by HPLC. Under these reaction conditions only HMFCA was observed in the solution. The dual chamber cell, consists of two compartments with a volume of 30 mL each, separated by an anionic membrane (HMED-0510-2, HUAMOTECH, China) (Extended Data Fig. 7). In this case oxygen was bubbled in one compartment and nitrogen in the other compartment for 20 min with a flow rate of 150 mL/min. While the oxygen was bubbling, the Pd/C electrode was rapidly introduced into the oxygen compartment and the Au/C electrode into the nitrogen compartment. The flow rate of each gas was reduced to 50 mL/min before connection of the electrodes and the start of the reaction. The same concentration of HMF (0.02 M) in the 0.1 M NaOH electrolyte were introduced into the two compartments to avoid any diffusion from one compartment to the other before the start of the reaction. At the end of each experiment, 0.2 mL of electrolyte solution was collected from each compartment and analysed by HPLC. Under these reaction conditions only HMFCA was produced in the solution. The protocol used for calculating the electron transfer efficiency in the short circuit current experiments is listed below:

Electron transfer efficiency (i.e. charge transfer) for single and dual cells[23]:

The moles of electrons, *i.e.,* n electrons, generated by the system was calculated using the equation below, where Q (C) is the amount of charge (A*s) generated during the time (s) of the reaction and F the Faraday constant (96485 C/mol):

$$(1)\ n(\text{electrons}) = Q/F$$

Q is obtained by integrating the curve (current *vs.* time) recorded during the reaction.

The stoichiometric moles of electrons generated during the reaction is twice the number of moles of HMFCA detected by HPLC, using the equations below.

$$(2)\ C_6H_6O_3\ (\text{HMF}) + 2OH^- \rightarrow C_6H_6O_4\ (\text{HMFCA}) + H_2O + 2e^-$$

$$(3)\ n(\text{electrons}) = 2 * n(\text{HMFCA})$$

The efficiency of electron transfer is the ratio between the measured moles of electrons flowing from the Au/C electrode to the Pd/C electrode (1) divided by the theoretical moles of electrons which should be generated from reaction stoichiometry based on the HPLC analysis of the products in the Au/C electrode compartment after reaction (2).

Electron transfer efficiency = (n(electrons) from (1) / n(electrons) from (3)) * 100

Catalyst Characterization

Scanning Transmission Electron Microscopy. Samples for examination by STEM were prepared by dry dispersing the catalyst powder onto a holey carbon film supported by a 300-mesh copper TEM grid. Bright field (BF) and high angle annular dark field (HAADF) STEM images were taken using an aberration corrected JEOL JEM ARM-200CF microscope at Lehigh University operating at 200 kV, equipped with a single JEOL Centurio silicon drift detector for X-ray energy dispersive spectroscopy (XEDS). The Au@Pd/C catalyst was analysed using a JEM ARM-200CF microscope equipped with dual Centurio silicon drift XEDS detectors at the in ePSiC facility at the Diamond Light Source (UK). The Au=Pd/C catalyst was analysed using a JEM ARM-200CF microscope equipped with Oxford Instruments X-MAX^N 100LTE XEDS detectors at the National University of Singapore. Particle size distribution histograms were generated by analysis of representative HAADF electron micrographs using Image J.

The geometric Mackay icosahedral model[24] was used to estimate the number of Au atoms associated with the entire particle volume and exposed particle surface, as a function of Au particle size. The table shows selected values of surface and total number of atoms from

Mackay icosahedra having different diameters. The particle diameter d was estimated using the equation $d = (2n + 1) \cdot 0.288$ (nm), where n is the number of shells in the Mackay model; the total atoms per particle (N_{total}) was calculated using the equation $N_{total} = \frac{10}{3}n^3 + 5n^2 + \frac{11}{3}n + 1$; the total number of exposed surface atoms ($N_{surface}$) was calculated using the equation $N_{total} = 10n^2 + 2$. The Mackay icosahedron chosen to best represent each binning interval was that which had the closest value to the median value of the binning interval.

Microwave plasma atomic emission spectroscopy: Reaction solutions were first filtered to remove heterogeneous catalyst from the sample. Further filtration was carried out using PTFE syringe filters (0.456 µm). The samples were then analysed using an Agilent MP-AES 4100 MP-AES spectrometer. Samples were investigated for the presence of precious metals (Au and Pd) using multiple wavelength calibrations for each individual element.

Inductively Coupled Plasma Mass Spectrometry: Reaction solutions were first filtered to remove any heterogeneous catalyst from the sample. Further filtration was carried out using PTFE syringe filters (0.456 µm). The samples were then analysed using an Agilent 7900 ICP-MS with an I-AS autosampler. A five-point calibration was conducted using Certified Reference material from Perkin Elmer and an Internal Standard also Certified from Agilent. All samples were diluted 10*x*; 500 µl of sample was added into a 5 mL class A volumetric with deionised H_20 (1% HNO_3 and 0.5% HCl matrix); the calibrants were matrix matched. Nickel sampling and skimmer cones were used for the analysis and He mode on the ORS4 Octopol to help with interference reduction.

Temperature Programmed Reduction:

Temperature programmed reduction (TPR) was performed on an Anton Paar, ChemBET. Samples (*ca*. 20 mg) were pre-treated in He (30 ml.min^{-1}) at 110 ^{o}C for 2 h. The TPR analysis was performed in 10% H_2/Ar (30 ml.min^{-1}) from 30 ^{o}C to 350 ^{o}C at 10 ^{o}C.min^{-1}.

X-ray Photoelectron Spectroscopy:

X-ray photoelectron spectroscopy (XPS) was performed on a Thermo Fisher Scientific K-alpha^{+} photoelectron spectrometer. Samples were mounted in small recesses within the Thermo Scientific copper powder plate. Samples were analysed using a micro-focused monochromatic Al X-ray source operating at 72 W (6 mA x 12 kV) using the 400 µm spot option, which is an

elliptical area of approximately 400 μm x 600 μm. Data was recorded at pass energies of 150 eV for survey scans and 40 eV for high resolution scan with 1 eV and 0.1 eV step sizes respectively. Charge neutralisation of the sample was achieved using a combination of both low energy electrons and argon ions which results in a C(1s) energy for the carbon support of 284.5 eV, typical of graphitic like carbons. Data analysis was performed in CasaXPS (v.2.3.24) using Scofield cross-sections with an energy dependence of -0.6 after removal of a Shirley background.

Method references

23. Ringeisen, B. R. *et al*. High power density from a miniature microbial fuel cell using shewanella oneidensis DSP10. *Environ. Sci. Technol.***40**, 2629-2634 (2006).

24. Mackay, A. L. A dense non-crystallographic packing of equal spheres. *Acta Cryst.* **15**, 916-918 (1962).

25. Siyo, B. *et al.* Influence of support on the aerobic oxidation of HMF into FDCA over preformed Pd nanoparticle based materials. *Appl. Catal. A, Gen.* **478**, 107–116 (2014).

26. Davis, S. E., Zope, B. N. & Davis, R. J. On the mechanism of selective oxidation of 5-hydroxymethylfurfural to 2,5-furandicarboxylic acid over supported Pt and Au catalysts. *Green Chem*. **14**, 143–147 (2012).

27. Han, X. *et al.* Base-free aerobic oxidation of 5-hydroxymethylfurfural to 2,5-furandicarboxylic acid over a Pt/C-O-Mg catalyst. *Green Chem.* **18**, 1597–1604 (2016).

28. Zhou, C. *et al.* Functionalized carbon nanotubes for biomass conversion: The base-free aerobic oxidation of 5-hydroxymethylfurfural to 2,5-furandicarboxylic acid over platinum supported on a carbon nanotube catalyst. *ChemCatChem*. **7**, 2853–2863 (2015).

29. Artz, J. & Palkovits, R. Base-free aqueous-phase oxidation of 5-hydroxymethylfurfural over ruthenium catalysts supported on covalent triazine frameworks. *ChemSusChem*. **8**, 3832–3838 (2015).

30. Mishra, D. K. *et al.* $MnCo_2O_4$ spinel supported ruthenium catalyst for air-oxidation of HMF to FDCA under aqueous phase and base-free conditions. *Green Chem.* **19**, 1619–1623 (2017).

31. Schade, O. *et al.* The influence of the gold particle size on the catalytic oxidation of 5-(hydroxymethyl)furfural. *Catalysts*. **10**, 342 (2020).

32. Megías-Sayago, C. *et al.* Effect of gold particles size over Au/C catalyst selectivity in HMF oxidation reaction. *ChemCatChem*. **12**, 1177–1183 (2020).

33. Ferraz, C. P. *et al.* 5-hydroxymethylfurfural and furfural base-free oxidation over AuPd embedded bimetallic nanoparticles. *Catalysts*. **10,** 75 (2020).

34. Yang, J. *et al.* Effect of the oxygen coordination environment of CaMn oxides on the catalytic performance of Pd supported catalysts for aerobic oxidation of 5-hydroxymethyl-2-furfural. Catal. Sci. Technol. **9**, 6659–6668 (2019).

35. Liu, Y. *et al.* Active oxygen species promoted catalytic oxidation of 5-hydroxymethyl-2-furfural on facet-specific Pt nanocrystals. *ACS Catal.* **9**, 8306–8315 (2019).

36. Megias-Sayago, C. *et al.* Understanding the role of the acid sites in 5-hydroxymethylfurfural oxidation to 2,5-furandicarboxylic acid reaction over gold catalysts: Surface investigation on $Ce_xZr_{1-x}O_2$ compounds. *ACS Catal.* **8**, 11154–11164 (2018).

37. Yu, K. *et al.* The role of Bi-doping in promoting electron transfer and catalytic performance of $Pt_{/3}$DOM-$Ce_{1-x}BixO_{2-\delta}$. *J. Catal.* **365**, 292–302 (2018).

38. Schade, O. R., Kalz, K. F., Neukum, D., Kleist, W. & Grunwaldt, J. D. Supported gold- and silver-based catalysts for the selective aerobic oxidation of 5-(hydroxymethyl)furfural to 2,5-furandicarboxylic acid and 5-hydroxymethyl-2-furancarboxylic acid. *Green Chem.* **20**, 3530–3541 (2018).

39. Masoud, N., Donoeva, B., de Jongh, P. E. Stability of gold nanocatalysts supported on mesoporous silica for the oxidation of 5-hydroxymethyl furfural to furan-2,5-dicarboxylic acid. *Appl. Catal. A* **561**, 150–157 (2018).

40. Wan, X. *et al.* Base-free aerobic oxidation of 5-hydroxymethyl-furfural to 2,5-furandicarboxylic acid in water catalyzed by functionalized carbon nanotube-supported Au-Pd alloy nanoparticles. *ACS Catal.* **4**, 2175–2185 (2014).

41. Bonincontro, D. *et al.* AuPd-nNiO as an effective catalyst for the base-free oxidation of HMF under mild reaction conditions. *Green Chem.* **21**, 4090–4099 (2019).

42. Gui, Z. *et al.* Efficient aerobic oxidation of 5-hydroxymethylfurfural in aqueous media with Au–Pd supported on zinc hydroxycarbonate. *ChemCatChem*. **8**, 3636–3643 (2016).

43. Kerdi, F. *et al.* Evaluation of surface properties and pore structure of carbon on the activity of supported Ru catalysts in the aqueous-phase aerobic oxidation of HMF to FDCA. *Appl. Catal. A* **506**, 206–219 (2015).

44. Ait Rass, H., Essayem, N. & Besson, M. Selective aerobic oxidation of 5-HMF into 2,5-furandicarboxylic acid with Pt catalysts supported on TiO_2- and ZrO_2-based supports. *ChemSusChem*. **8**, 1206–1217 (2015).

45. Chen, H. *et al.* Atomic layer deposition of Pt nanoparticles on low surface area zirconium oxide for the efficient base-free oxidation of 5-hydroxymethylfurfural to 2,5-furandicarboxylic acid. *Appl. Catal. A* **555**, 98–107 (2018).

Acknowledgments

We thank L. Kang and R. Wang from University College London and Cardiff University for access and assistance with the electron microscopy. We thank the Diamond Light Source for access to beamline E01 (proposal number EM18909). C.J.K. gratefully acknowledges funding from the National Science Foundation Major Research Instrumentation program (GR# MRI/DMR-1040229). S. M. A thanks the Saudi Arabian government for his PhD scholarship. X. Y. H and Q. H would like to thank Cardiff University School of Chemistry for financial support. Q. H. would also like to acknowledge the support by National Research Foundation (NRF) Singapore, under its NRF Fellowship (NRF-NRFF11-2019-0002). K.W. and L. Z. would like to express gratitude to the Chinese Scholarship Council (CSC) for financial support. XPS data collection was performed at the EPSRC National Facility for XPS ('HarwellXPS'), operated by Cardiff University and UCL, under contract No. PR16195. We thank Cardiff University and the Max Planck Centre for Fundamental Heterogeneous Catalysis (FUNCAT) for financial support.

Author Contributions

X.Y.H., O.A., M.D., R.J.L., S.P., P.J.M., and G.J.H. contributed to the design of the study; X.Y.H., O.A., L.Z., I.T.D., R.J.L., K.W., J.F. and F.W. conducted experiments and data analysis. O.A. and X.Y.H. conceived the mechanism; X.Y.H., O.A, M.D., R.J.L., S.P., P.J.M., G.S., D.B., S.M., C.J.K., and G.J.H. provided technical support, conceptual advice and result interpretation. X.Y.H., O.A., S.P., G.S. D.J.M., S.M.A., T.E.D., Q.H., and C.J.K. conducted catalyst characterization and corresponding data processing. M.D., O.A., D.B. and G.J.H. wrote the manuscript; X.Y.H. wrote the extended data figures and tables. X.Y.H., O.A., M.D., R.J.L., S.P., G.S., D.B., S.M., C.J.K. and G.J.H commented on- and amended both documents. All authors discussed and contributed to the work.

Competing Interests

All authors declare no competing interests.

Data and materials availability: All data needed to evaluate the conclusions in the paper are present in the paper or the extended data.

Corresponding Authors

Graham J. Hutchings is the sole corresponding author affiliated with this work. Correspondence and requests for materials should be addressed to Graham J. Hutchings.

Email: hutch@cardiff.ac.uk

Extended Data Figures and Tables

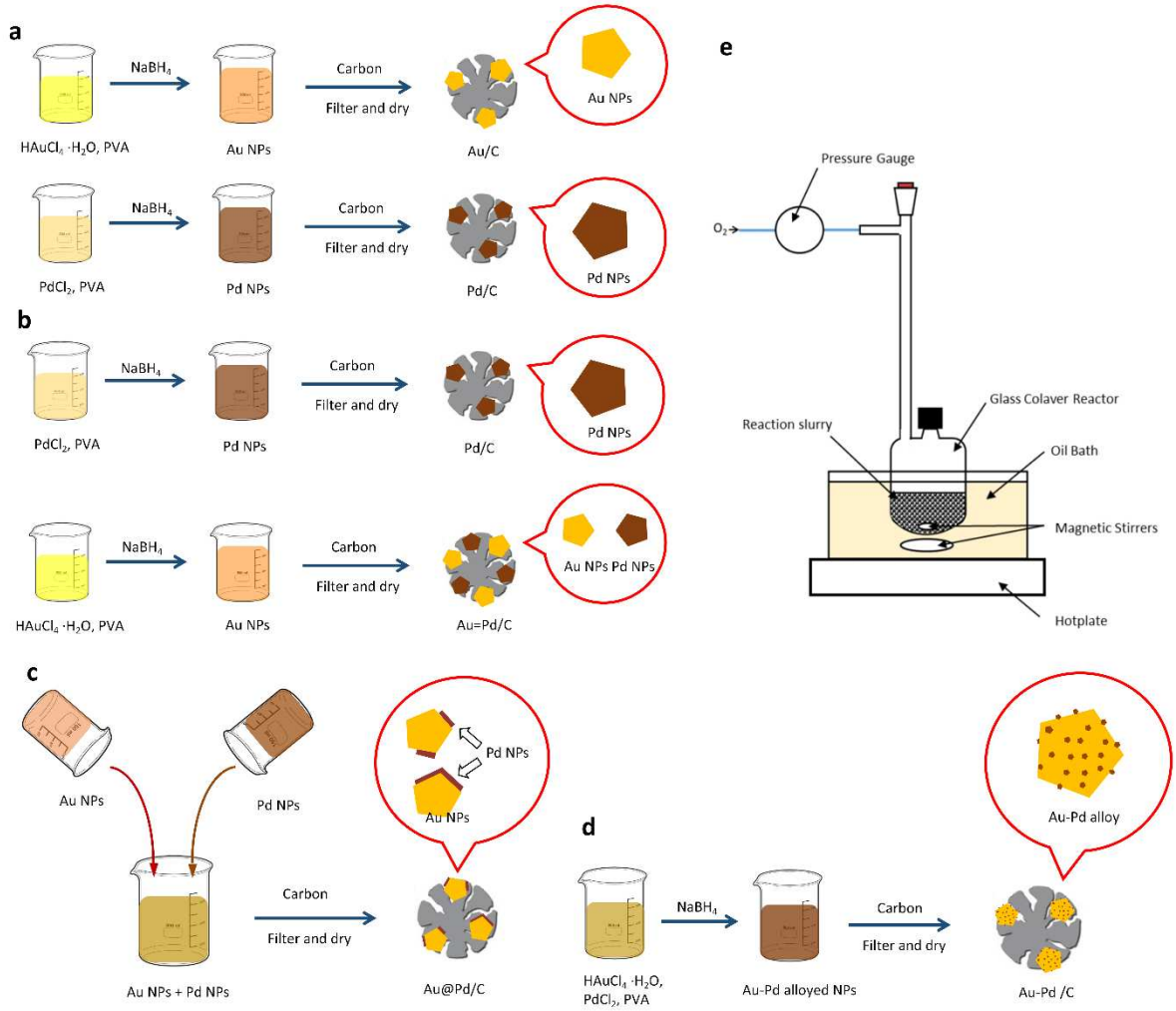

Extended Data Fig. 1 | Diagrammatic representation of the sol-immobilisation method used for catalyst preparation. **a**, monometallic Au/C and Pd/C. **b**, Au=Pd/C. **c**, Au@Pd/C catalysts**. d**, alloyed Au-Pd/C. **e**, schematic representation of our reactor set-up for the thermocatalytic experiments.

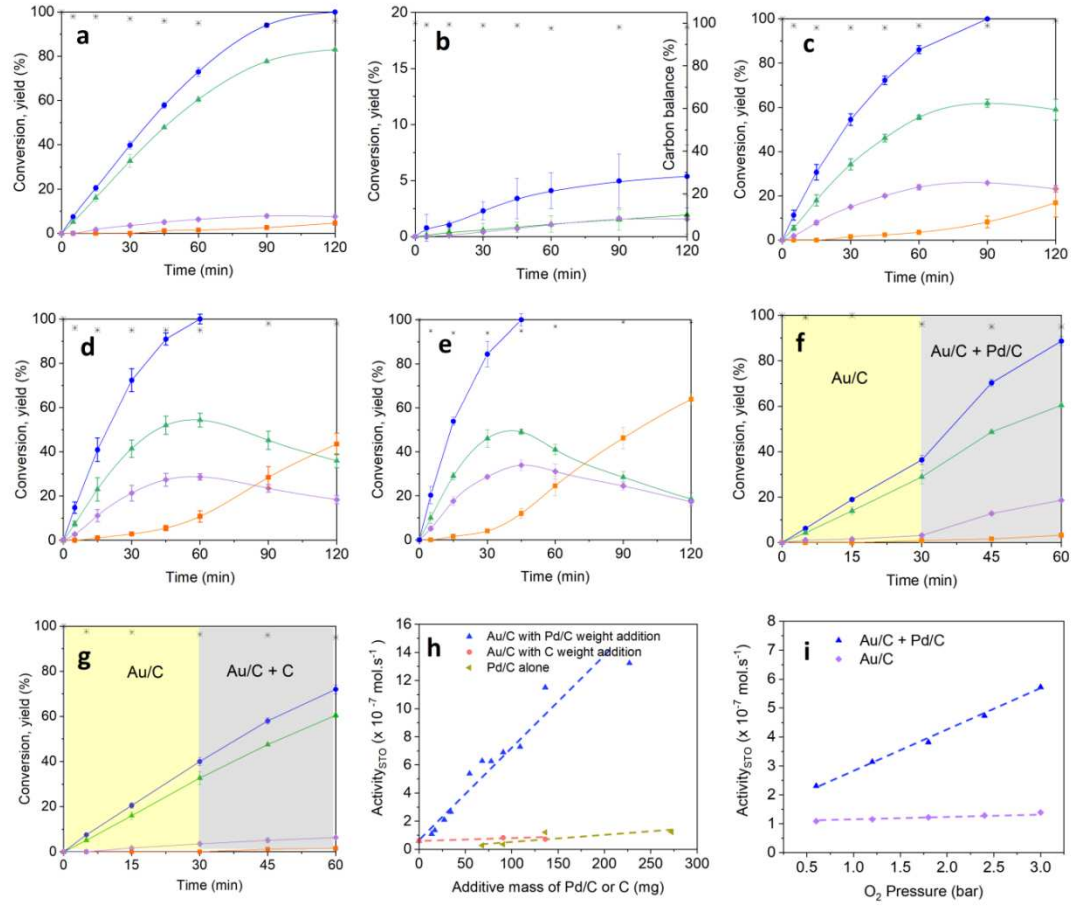

j Catalyst	Conversion (%)	ODH Rate (mol . L^{-1} . s^{-1})	Mean Particle Size (nm)	TOF (s^{-1})
Au/C	7.5	2.5 x 10^{-5}	3.12	0.169
Pd/C	0.8	2.7 x 10^{-6}	3.40	0.068
Au-Pd/C	11.3	3.8 x 10^{-5}	2.80	0.228
Au/C +Pd/C	14.7	4.9 x 10^{-5}	See entries 1 and 3	0.262
Au@Pd/C	20.2	6.7 x 10^{-5}	3.87	0.464

Extended Data Fig. 2 | Time-on-line data of aqueous HMF oxidation over series of Au/Pd catalysts and their TOF. a, Au/C. b, Pd/C. **c,** Au-Pd/C alloy. **d,** physical mixture of Au/C + Pd/C. **e,** Au@Pd/C. **f,** Au/C followed by the addition of Pd/C after 30 min. **g,** Au/C followed by the addition of C after 30 min. Reaction conditions: HMF (0.1 M); $NaHCO_3$ (0.4 M); H_2O (16 mL); Au/C: 72.1 mg; Pd/C: 71 mg; Au-Pd/C alloy: 143.1 mg; Au@Pd/C: 143.1 mg; C: 71 mg; 80 °C; pO_2 = 3 bar. Key: FDCA yield (■), FFCA yield (◆), HMFCA yield (▲), HMF conversion (●), mass balance (*). Associated error bars correspond to mean +/- SD (N = 5). **h**, The influence on ODH activity when various quantities of Pd/C (▲) and C (●) are added to Au/C (72.1 mg); ODH activity exhibited by various quantities of Pd/C, in the absence of Au/C, is also displayed (◀). **i**, the influence of oxygen pressure (0.6 – 3.0 bar) on ODH activity over a physical mixture of Au/C + Pd/C (▲) and Au/C (♦) is displayed. The reaction conditions used for h and i are displayed in the Method section. **j**, summary of each catalyst in terms of HMF conversion, initial rate and TOF at a 5 min reaction time. The total active sites available in each catalyst was estimated using the Mackay model, based on the presented particle size distributions[s]. Further information relating to how the TOF's were calculated, can be found in the Methods section.

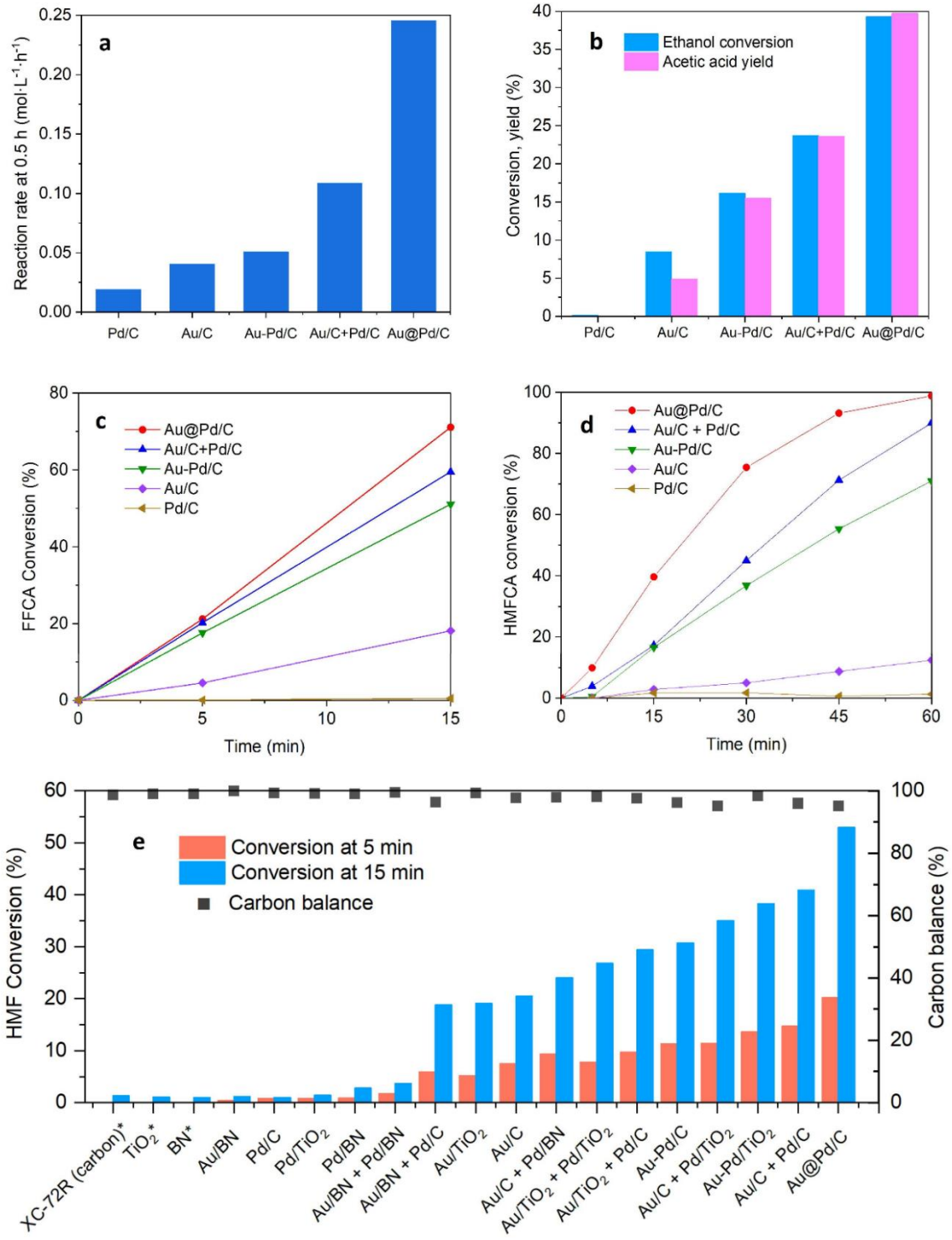

Extended Data Fig. 3 | Catalytic performance over Au/C, Pd/C, Au-Pd/C alloy, Au/C + Pd/C physical mixture and Au@Pd/C catalysts in series of alcohol oxidation reactions. **a**, glycerol oxidation. **b**, ethanol oxidation. **c**, 5-formyl-2-furancarboxylic acid (FFCA) oxidation and **d**, 5-hydroxymethylfuroicacid (HMFCA) oxidation. Reaction conditions were all listed in the Method section. **e**, Conversion values for the HMF oxidation reaction after 5 and 15 min time-on-line for the various catalysts studied in this work. Reaction conditions: HMF (0.1 M); $NaHCO_3$ (0.4 M); H_2O (16 mL); Au/(C/TiO_2/BN): 72.1 mg, Pd/(C/TiO_2/BN): 71 mg, Au@Pd/C, Au-Pd/(C/TiO_2/BN) and Au/(C/TiO_2/BN) + Pd/(C/TiO_2/BN): 143.1 mg; 80 °C; pO_2 = 3 bar; reaction time: 15 min. * presents the test on bare supports in HMF oxidation, HMF (0.1 M); $NaHCO_3$ (0.4 M); H_2O (16 mL); C/TiO_2/BN: 60 mg; 80 °C; pO_2 = 3 bar; reaction time: 30 min.

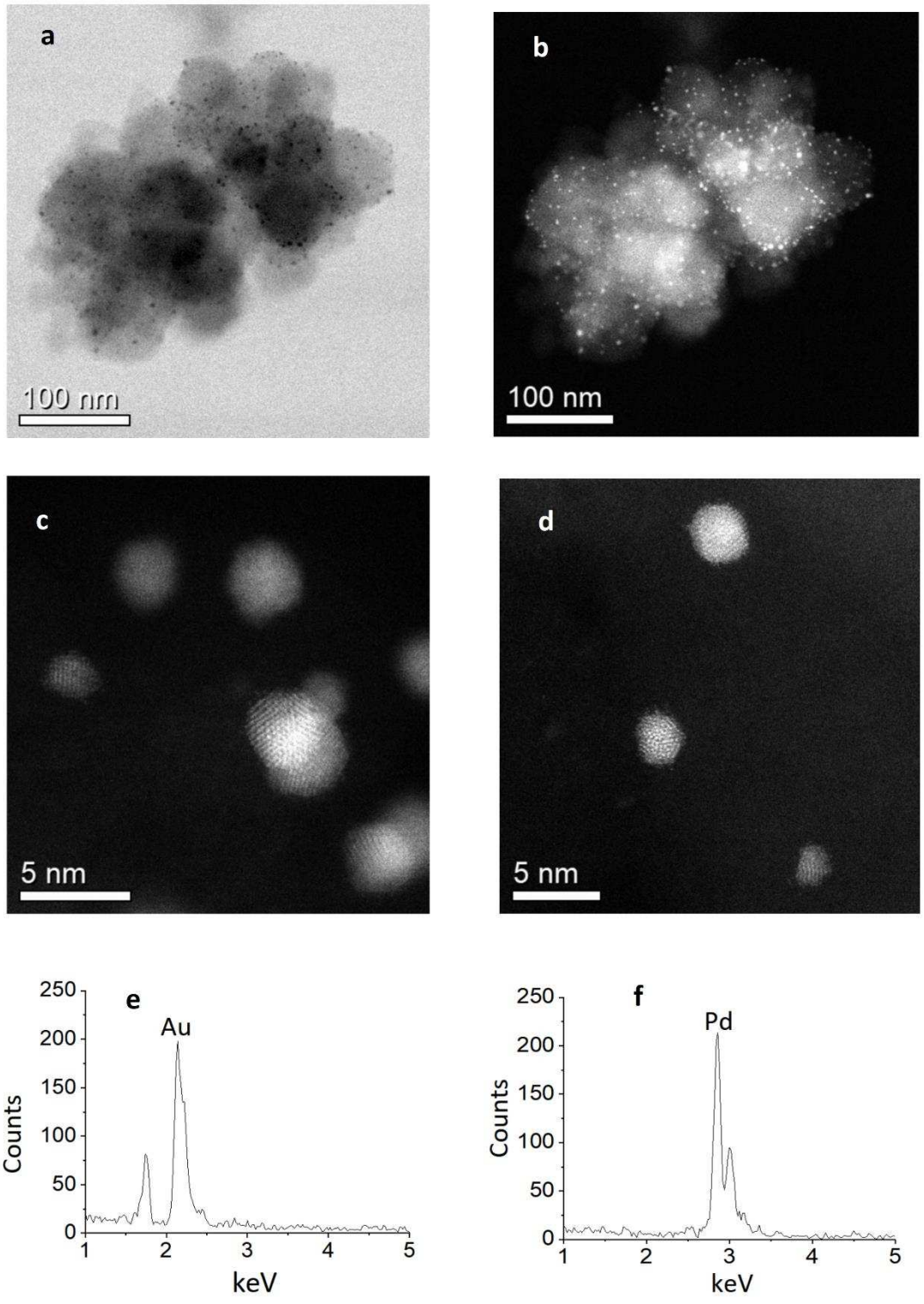

Extended Data Fig. 4 | Electron microscopy analysis of Au/C + Pd/C (physical mixture) catalyst after one cycle of use in the oxidation of HMF. **a** and **b**, Representative complementary BF- and HAADF-STEM micrographs showing metal nanoparticle size and spatial distribution. **c**, Atomic resolution HAADF-STEM micrograph of a C grain supporting Au particles and **d**, a C grain supporting Pd particles confirming that the Au and Pd remain separated under our reaction conditions. **e** and **f**, are representative XEDS spectra of individual Au particles and Pd particles in the catalyst, respectively. No evidence was observed of Au or Pd migration or intermixing after the catalytic reaction.

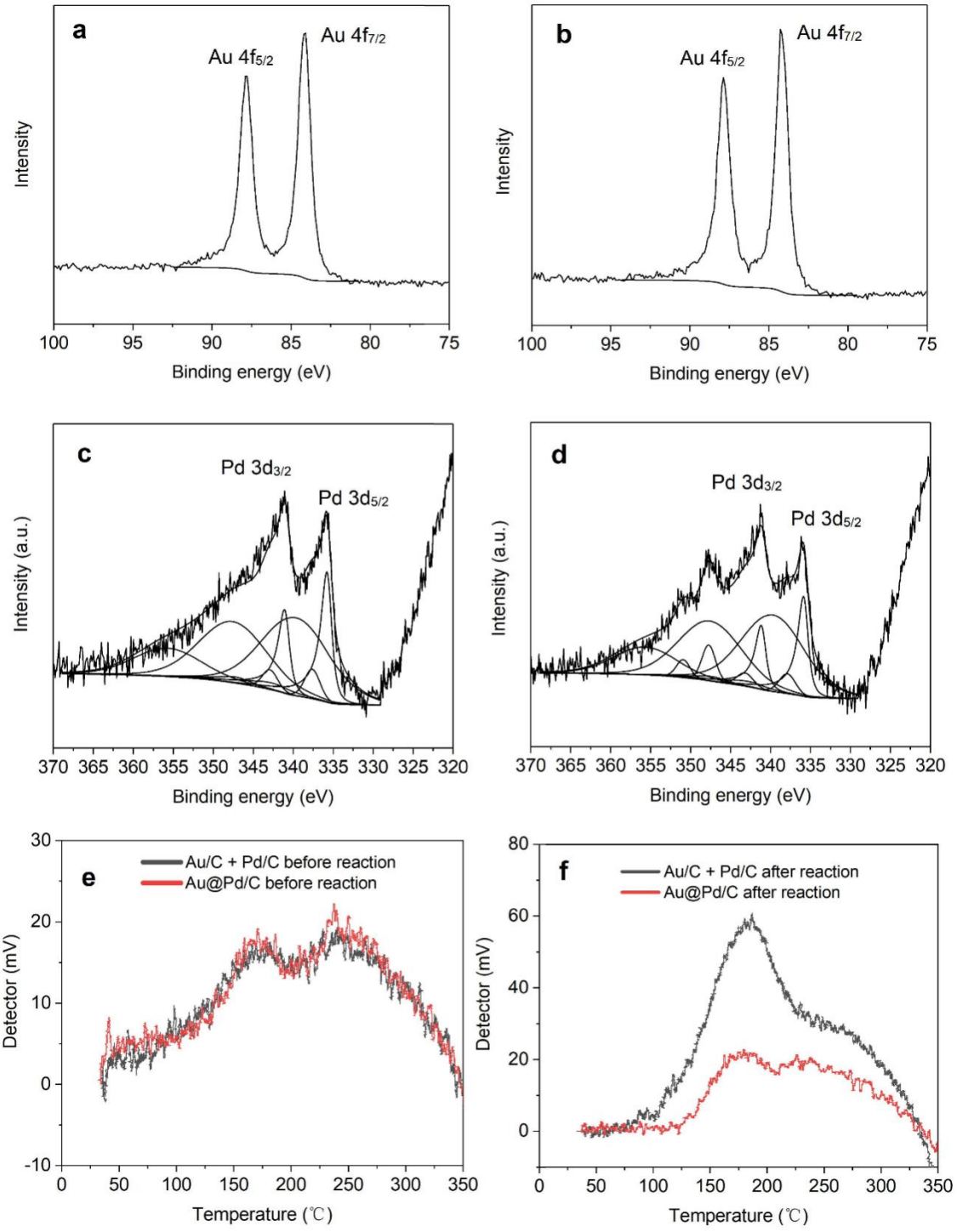

Extended Data Fig. 5 | X-ray photoelectron spectroscopy (XPS) data. **a** and **b**, Au 4f and **c** and **d**, Pd 3d /Au 4d regions for Au/C and Pd/C monometallic catalysts before and after a typical HMF oxidation reaction as a physical mixture. Among which, a, fresh Au/C; b, used Au/C; c, fresh Pd/C and d, used Pd/C. Temperature programmed reduction data for the physically mixed Au/C + Pd/C catalyst and the Au@Pd/C catalyst **e**, before and **f**, after HMF oxidation.

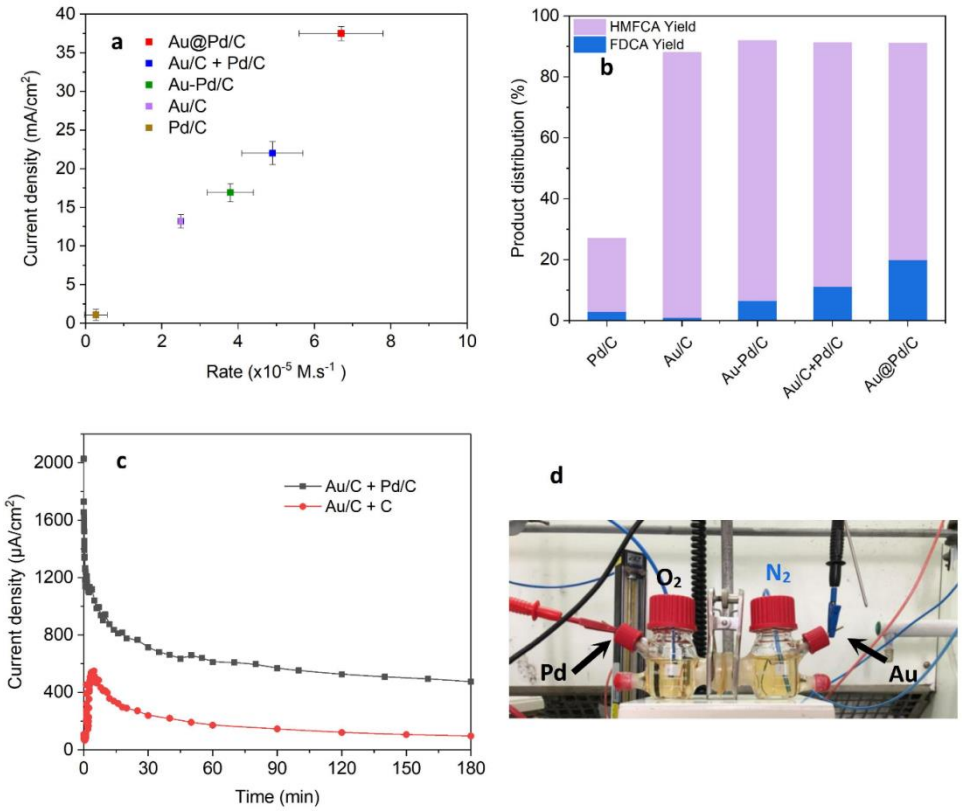

e

Catalyst	Cell type	Reaction time (min)	HMFCA yield (x 10^{-6} mol)
Au/C[i]	Single cell	120	0.50
Au/C[ii]	Single cell	120	2.51
Au/C + Pd/C[ii]	Single cell	180	7.64
Au/C + Pd/C[iii]	Dual cell	120	2.98
Au/C + Pd/C[iv]	Dual cell	120	1.50
Au/C + doubled	Dual cell	90	2.16

Extended Data Fig. 6 | Electrochemical and thermal catalytic oxidation of aqueous HMF over Au/Pd catalysts. **a**, Correlation between the thermo- and electro-catalytic HMF oxidation experiments over the series of catalysts. For the thermocatalytic experiments, the initial rate measurements were taken after 5 minutes of reaction. The current density measurements were taken from the maxima observed in the corresponding CV experiments (Fig. 3a). Associated error bars correspond to mean +/- SD (N = 3). **b**, Aqueous HMF oxidation over series of mono- and bi-metallic Au-Pd catalysts. Reaction conditions: HMF (0.1 M); NaOH (0.4 M); H_2O (16 mL); 25 °C; pO_2 = 3 bar; 30 min; catalyst amounts for Au@Pd/C, Au/C + Pd/C and Au-Pd/C:143.1 mg, Au/C: 72.1 mg, Pd/C: 71 mg, carbon balance: ca 92%. **c**, Catalytic performance in short circuit with current density (normalized by an electrode surface area of 0.07 cm^2) generated as a function of time in the single chamber cell. Reaction conditions: 0.1 M NaOH and 0.02 M of HMF in 50 mL H_2O; Au (working electrode) and Pd or C (counter electrode); 25 °C; O_2 flow: 50 mL/min. **d**, H-type dual cell, consisting of Au as the anode in an N_2 flow, and Pd as cathode in an O_2 flow. The two cells are connected via an anion exchange membrane. Reaction conditions: each cell contains 0.1 M NaOH and 0.02 M of HMF in 35 mL H_2O; 25 °C; gas flow O_2/N_2: 50 mL/min. **e**, Reaction conditions: i: 0.1 M NaOH and 0.02 M of HMF in 50 mL H_2O, 25 °C, N_2 flow: 50 mL/min; ii: 0.1 M NaOH and 0.02 M of HMF in 50 mL H_2O, 25 °C, O_2 flow: 50 mL/min; iii: each cell consists of 0.1 M NaOH and 0.02 M of HMF in 35 mL H_2O, 25 °C, O_2/N_2 flow: 50 mL/min; iv: same to iii, except for the electrodes of Au and Pd are disconnected; v: same as iii, except for the Pd/C amount is doubled.

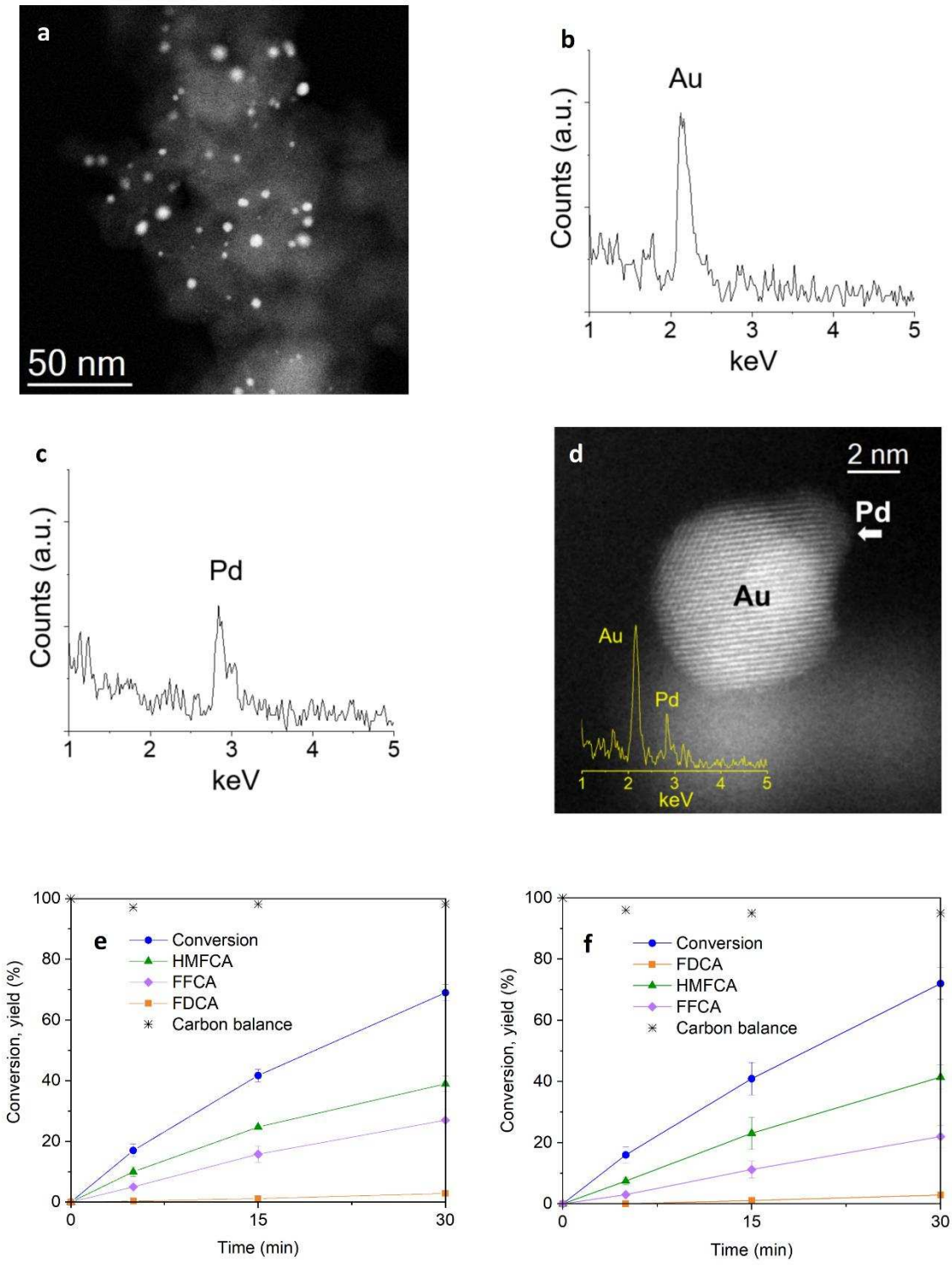

Extended Data Fig. 7 | Representative STEM-HAADF images and X-ED Spectra of nanoparticles in the Au=Pd/C catalysts and its corresponding activities. **a**, Lower magnification STEM-HAADF image of the Au=Pd/C catalyst. **b** and **c**, X-ED spectra obtained from individual nanoparticles, showing a Au-only and a Pd nanoparticle. **d**, STEM-HAADF image and the corresponding X-ED spectrum (inlet) of a Janus-like particle occasionally found in this Au=Pd/C catalyst. **e**, Activity comparison to the physical mixture **f**. Reaction conditions: HMF (0.1 M); $NaHCO_3$ (0.4 M); H_2O (16 mL); Au/C: 72.1 mg; Pd/C: 71 mg; Au=Pd/C: 143.1 mg; 80 °C; pO_2 = 3 bar; Reaction time: 30 min. Associated error bars correspond to mean +/- SD (N=3).

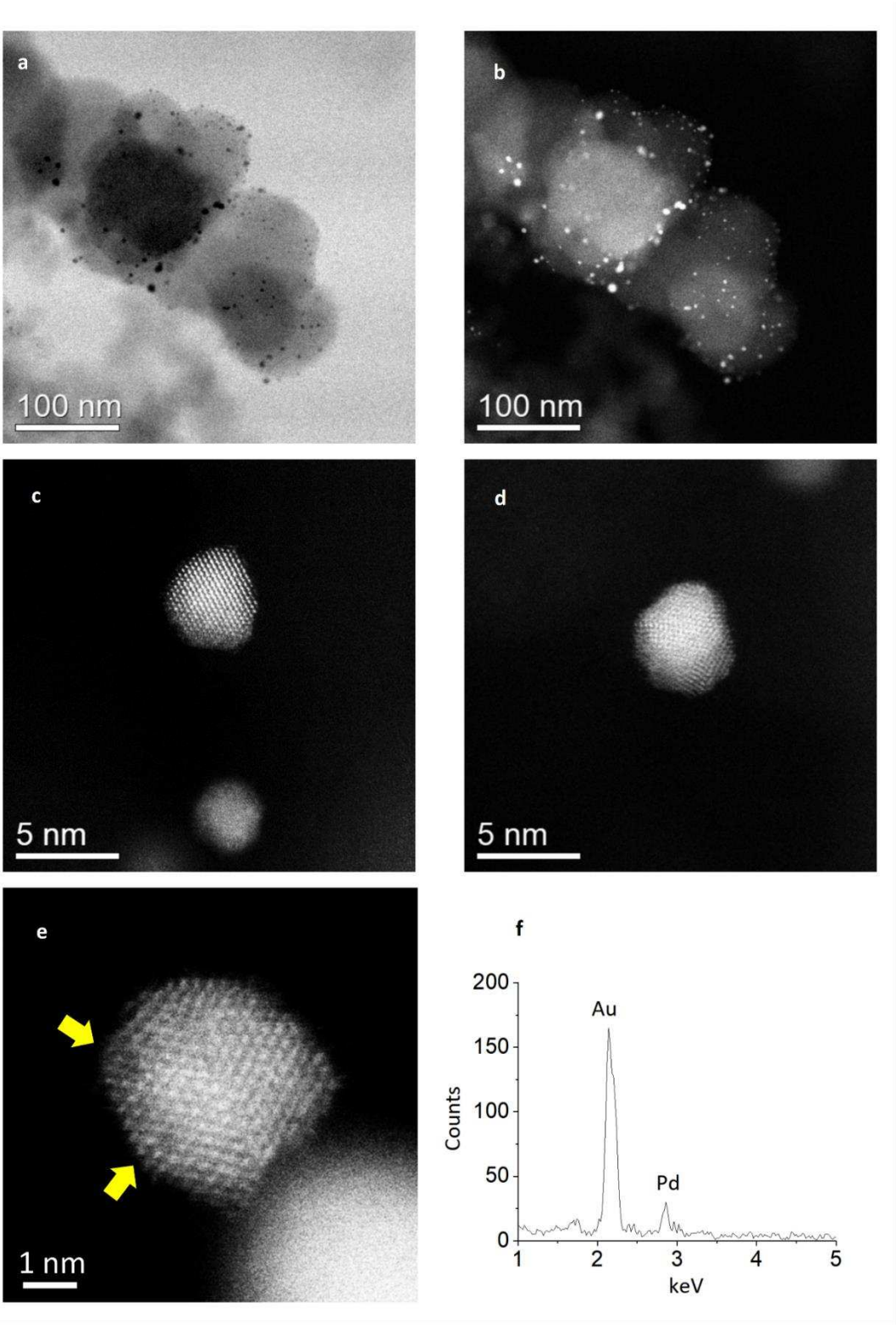

Extended Data Fig. 8 | Electron microscopy analysis of Au@Pd/C catalyst after one cycle of use in the oxidation of HMF. **a** and **b**, Representative complementary pair of BF- and HAADF-STEM micrographs showing metal nanoparticle size and spatial distribution. **c-e**, show atomic resolution HAADF-STEM micrographs of particles. The yellow arrows in e highlight certain atomic columns that appear lower in contrast, indicating some alloying of Pd with the Au matrix. **f**, A representative XEDS spectrum obtained from a typical nanoparticle, showing the presence of both Au and Pd.

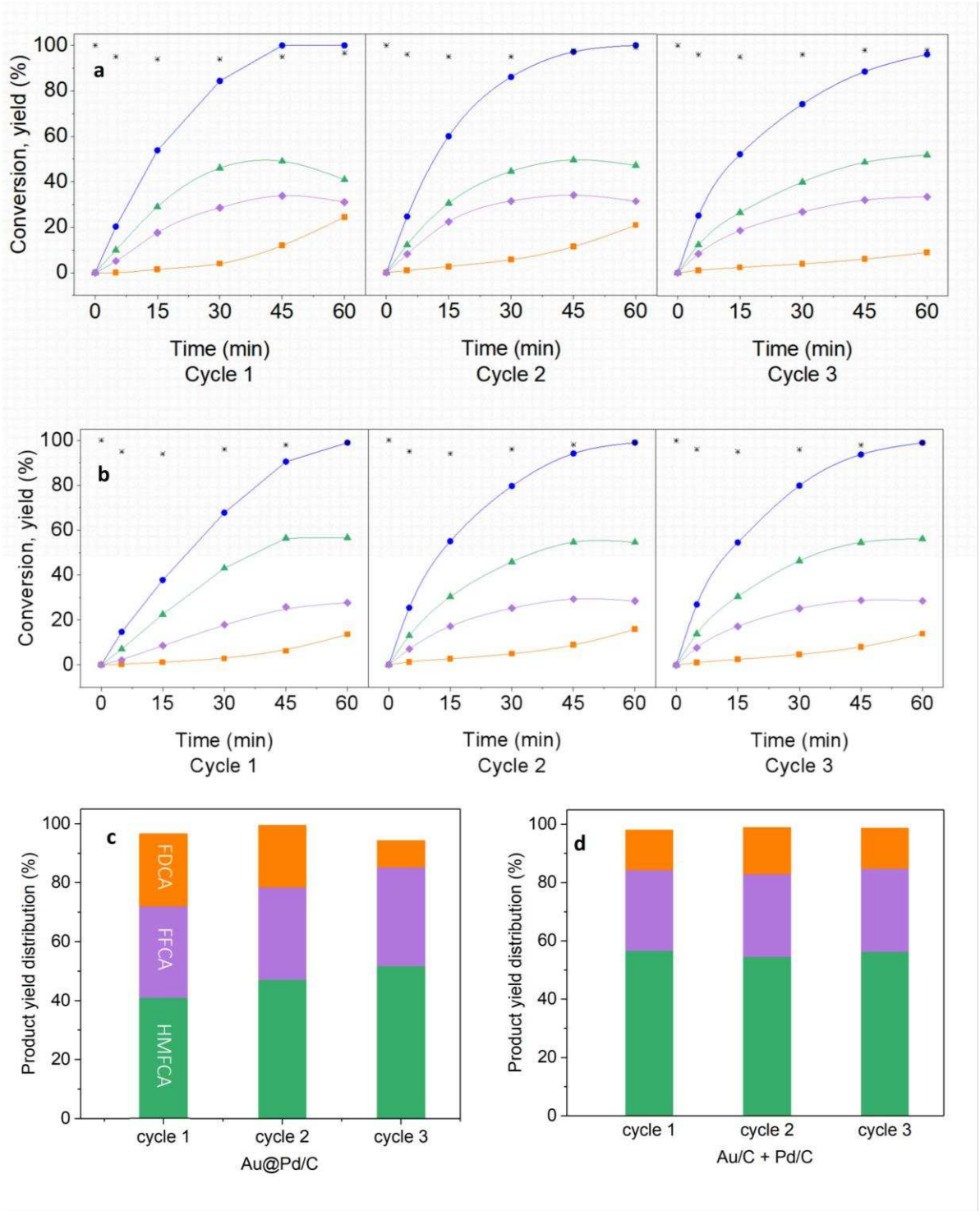

Extended Data Fig. 9 | Reusability data for the prepared Au/Pd catalysts in HMF oxidation reaction. **a** and **c**, The Au@Pd/C catalyst. **b** and **d**, the physical mixture Au/C + Pd/C catalyst. Reaction conditions: HMF (0.1 M); $NaHCO_3$ (0.4 M); H_2O (16 mL); Au@Pd/C: 143.1 mg; 80 °C; pO_2 = 3 bar; reaction time: 60 min. Key: FDCA yield (■), FFCA yield (◆), HMFCA yield (▲), HMF conversion (●), mass balance (*).

Extended Data Table 1 | The performance of supported metal catalysts in the aqueous phase aerobic oxidation of 5-hydroxymethyl furfural to furan dicarboxylic acid (FDCA).

Catalyst	Base / Quantity (mmol)	HMF/metal (mol/mol)	*T* (°C) / *t* (h)	Solvent / Volume (mL)	O_2 Pressure (Bar)	FDCA Productivity (mol_{FDCA} . mol_{metal} .h^{-1})	Reference
Au/TiO_2	NaOH/15.0	100/1	22 / 22	H_2O / 5	3.45	3.6	*14*
Pt/C	NaOH/1.5	150/1	22 / 6	H_2O / 5	3.45	17.0	*14*
$Pd/ZrO_2/LaO_2$	NaOH /10.0	100/1	90 / 4	H_2O / 20	Bubbled (35 mL min^{-1})	6.04	25
$Pd/KF/Al_2O_3$	NaOH / 0.5	100/1	90 / 7	H_2O / 20	Bubbled (35 mL min^{-1})	13.0	25
Au–Pd/AC	**NaOH/6.0**	**200/1**	**60 / 2**	**H_2O / 20**	**3.00**	**98.0**	*26*
Pt/C–O–Mg	—	50/1	110 / 12	H_2O / 10	10.00	4.0	27
Pt/CNT	—	100/1	95 / 12	H_2O / 20	5.00	7.0	*28*
Ru/CTF	—	40/1	140 / 1	H_2O / 15	4.00	31.2	29
$Ru/MnCo_2O_4$	—	214/1	120 / 10	H_2O / 20	4.80	3.3	30
Au/ZrO_2	NaOH / 4.0	100/1	100 / 5	H_2O/ 10	2.00	9.6	31
Au/C	NaOH/ 4.0	100/1	70 / 4	H_2O / 25	10.00	23.0	32
$Au_4Pd_1/SiTi$	—	18/1	100 / 24	H_2O / 2	1.00	0.1	33
$Pd/CaMn_2O_4$	Na_2CO_3 / 0.8	25/1	100 / 3	H_2O / 10	Bubbled (100 mL min^{-1})	5.8	34
Cubic Pt-nanocrystals	$NaHCO_3$ / 0.8	50/1	100 / 4	H_2O / 10	Bubbled (75 mL min^{-1})	7.3	35
Au/Ce25Zr	NaOH / 4.0	100/1	70 / 4	H_2O / 25	10.00	20.0	*36*
Pt/3DOM-$Ce_{0.8}Bi_{0.2}O_{2-\delta}$	$NaHCO_3$ / 1.6	100/1	90 / 10	H_2O / 20	Bubbled (70 mL min^{-1})	10.6	37
Au/ZrO_2	NaOH / 4.0	125/1	100 / 5	H_2O / 10	2.00	18.8	38
Au/SiO_2	$NaHCO_3$ / 0.4	72/1	90 / 6	H_2O / 8	10.00	8.8	39
AuPd/MgO	—	100/1	100 / 12	H_2O / 20	5.00	8.3	40
AuPd/CNT	—	100/1	100 / 12	H_2O / 20	5.00	7.2	40
AuPd-nNiO	—	100/1	90 / 6	H_2O / 25	10.00	11.5	41
AuPd/ZOC	$NaHCO_3$ / 2.0	100/1	80 / 4	H_2O / 10	3.00	24.8	42
Ru/AC	$NaHCO_3$ / 30.0	100/1	100 / 48	H_2O / 150	8.00	1.9	43
Pt/TiO_2	$NaHCO_3$ / 60.0	100/1	100 / 12	H_2O / 150	8.00	7.9	44
[x] $BiPt/TiO_2$	$NaHCO_3$ / 60.0	100/1	100 / 10	H_2O / 150	8.00	9.9	44
$Pt-ZrO_2$	—	72/1	100 / 4	H_2O / 3	4.00	5.8	45
Au/C	$NaHCO_3$ / 6.4	200/1	80 / 2	H_2O / 16	3.00	6.3	
Pd/C	$NaHCO_3$ / 6.4	200/1	80 / 2	H_2O / 16	3.00	0.0	
Au/C + Pd/C	$NaHCO_3$ / 6.4	200/1	80 / 2	H_2O / 16	3.00	43.5	
Au-Pd/C	$NaHCO_3$ / 6.4	200/1	80 / 2	H_2O / 16	3.00	17.0	**This Work**
Au@Pd/C	$NaHCO_3$ / 6.4	200/1	80 / 2	H_2O / 16	3.00	64.0	
* Au/C + Pd/C	$NaHCO_3$ / 6.4	200/1	80 / 2	H_2O / 16	3.00	54.4	
* Au-Pd/C	$NaHCO_3$ / 6.4	200/1	80 / 2	H_2O / 16	3.00	21.3	
* Au@Pd/C	$NaHCO_3$ / 6.4	200/1	80 / 2	H_2O / 16	3.00	80.0	

* Productivity calculated based on moles of Au only

[x] Productivity calculated based on moles of Pt only